Non-local real-space diffusion-driven models for microstructural evolution of irradiated tungsten.

S.L. Dudarev[1], D.R. Mason[1], D. Nguyen-Manh[1], I. Rovelli[1,2], A.E. Sand[3], A.P. Sutton[2] , T.D. Swinburne[1,4], J. Wrobel[5]

[1]CCFE, UK Atomic Energy Authority, Oxfordshire, UK.
[2]Department of Physics, Imperial College London, UK.
[3]Department of Physics, University of Helsinki, Finland.
[4]Theoretical Division T-1, Los Alamos National Laboratory, USA
[5]Warsaw University of Technology, Poland

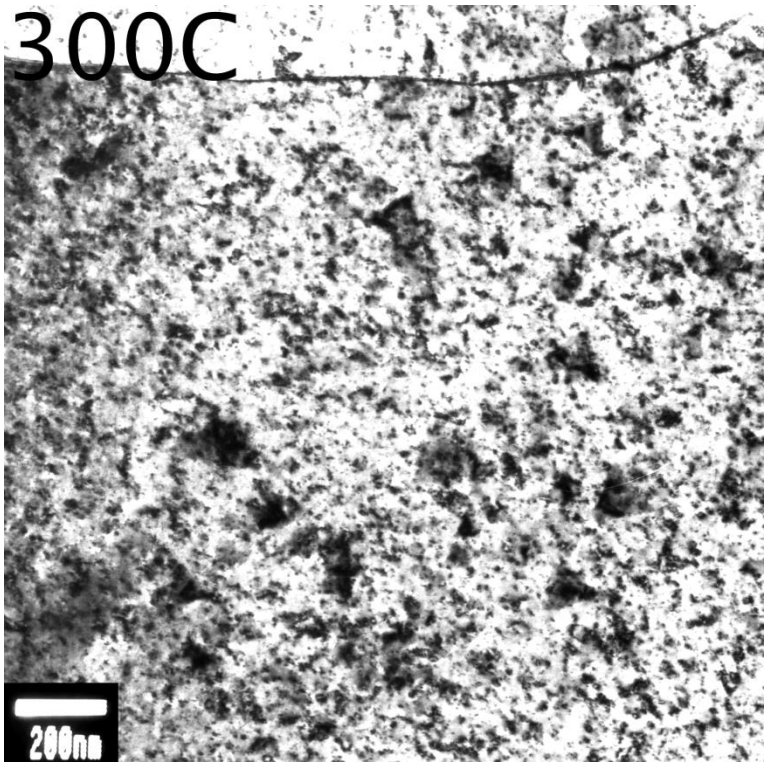

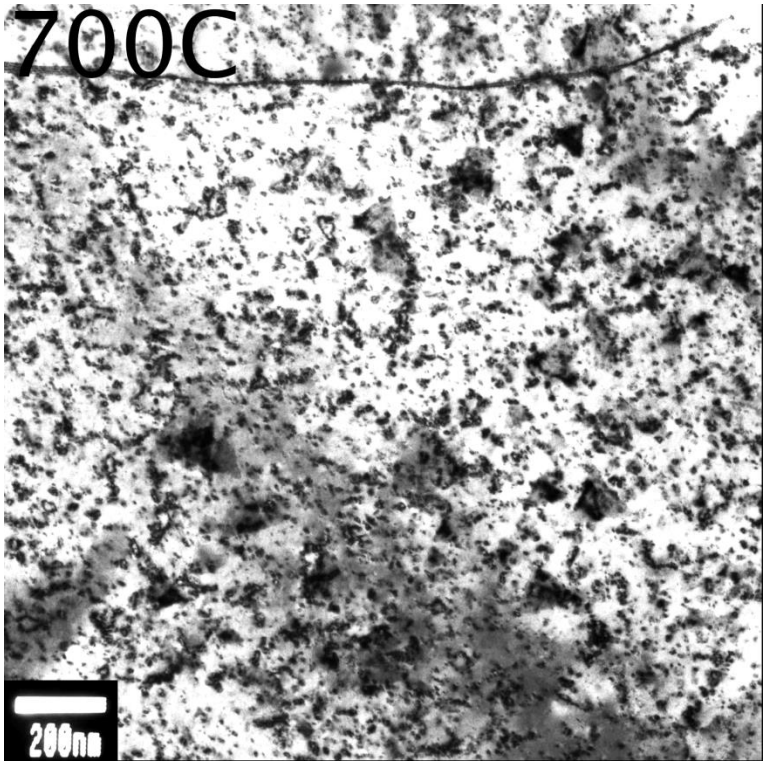

Francesco Ferroni, Xiaoou Yi, Kazuto Arakawa *et al*., High temperature annealing of ion irradiated tungsten, Acta Mater. **90** (2015) 380–393

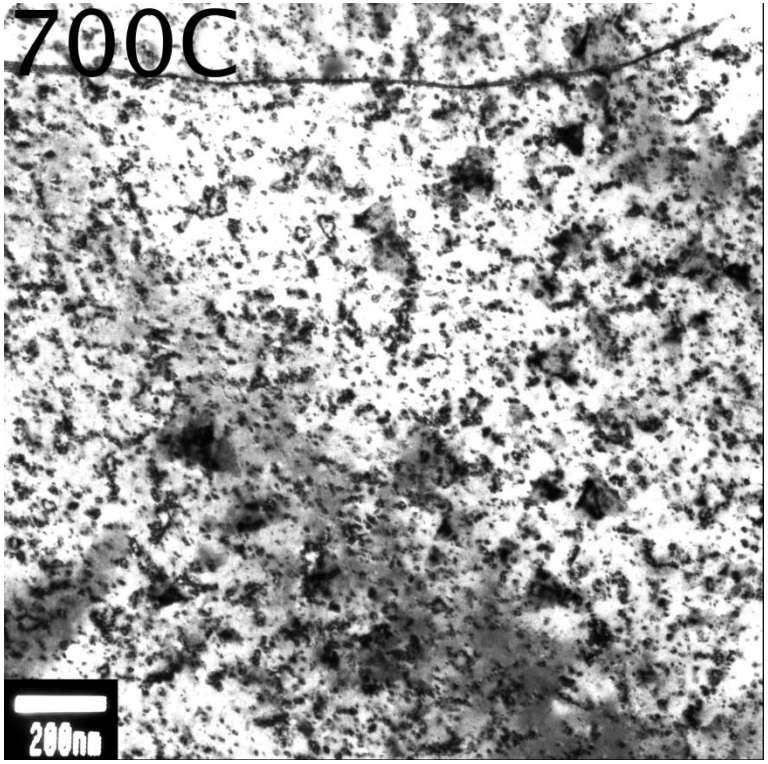

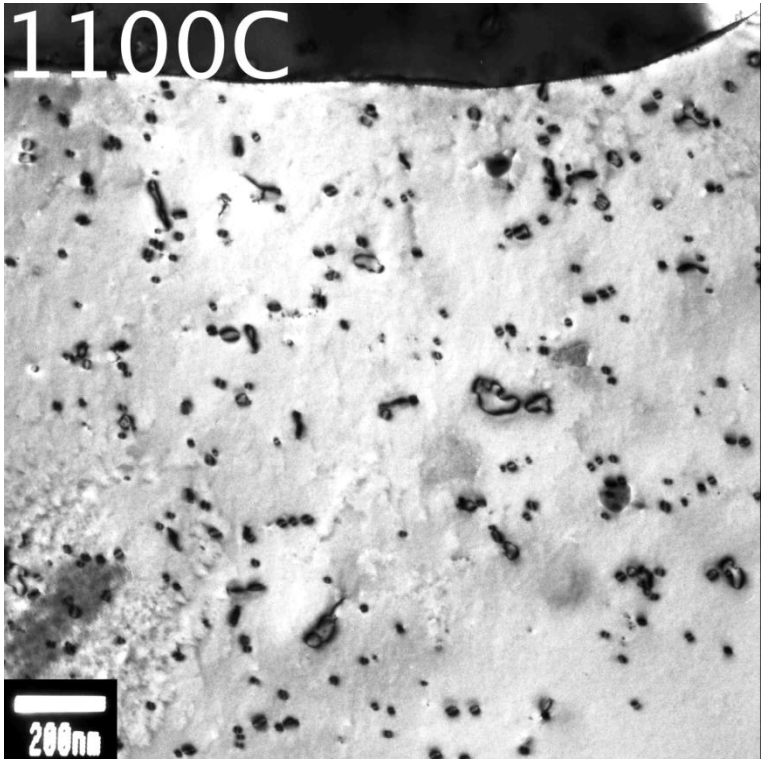

Francesco Ferroni, Xiaoou Yi, Kazuto Arakawa *et al*., High temperature annealing of ion irradiated tungsten, Acta Mater. **90** (2015) 380–393

Francesco Ferroni, Xiaoou Yi, Kazuto Arakawa *et al*., High temperature annealing of ion irradiated tungsten, Acta Mater. **90** (2015) 380–393. The movie shows the dynamics of recovery of defects in tungsten at 1100ºC.

OUTLINE

1. Production of defects in collision cascades in tungsten.

2. High and low-temperature mobility of radiation defects.

3. Diffusion-mediated models for microstructural evolution:
    1. Self-diffusion of dislocations
    2. Vacancy-diffusion-mediated evolution

4. Anomalous phase decomposition of W-Re alloys

Defect production in tungsten

The maximum cascade energy is (a non-relativistic estimate assuming a head-on elastic neutron-atom impact)

$$E_{\max} \approx \frac{4 m_n M_W}{(m_n + M_W)^2} E_n \approx 300\ \text{keV};$$

$$E_n = 14.1\ \text{MeV}$$

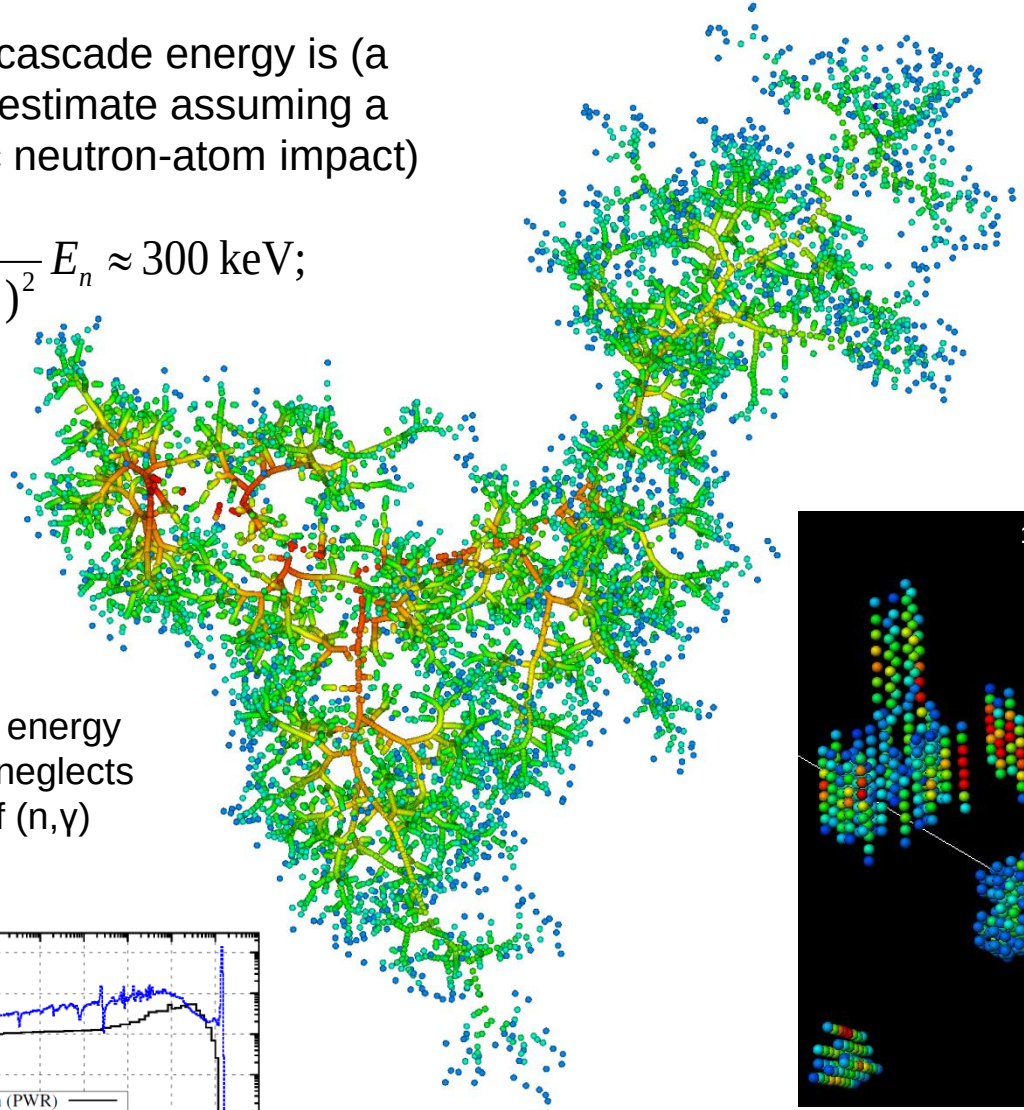

A 150 keV collision cascade in tungsten

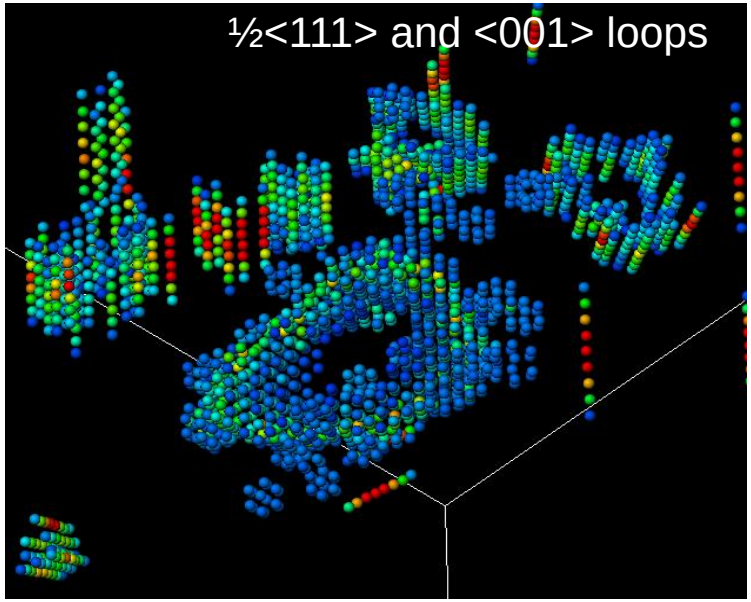

A.E. Sand *et al.*, EPL **103** (2013) 46003

Average cascade energy is ~150 keV [this neglects the contribution of (n,γ) reactions]

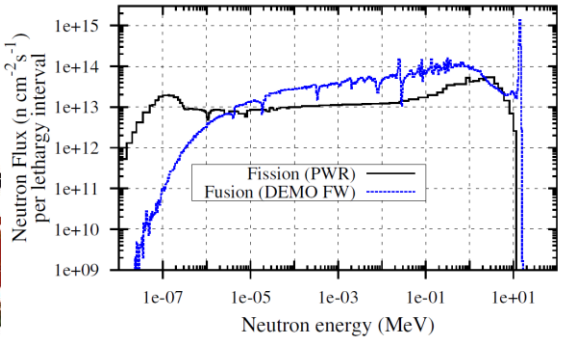

Defect production: fundamentals

1. Given arbitrarily high energy of the initial ion/neutron impact, is it possible to produce a defect cluster of arbitrarily large size directly in a cascade event?

2. The “dark matter” question: how many defects produced in cascades remain invisible to transmission electron microscopy and other high-resolution methods, and what is their effect on microstructure?

A.E. Sand *et al.* EPL **103** (2013) 46003; D.R. Mason *et al.*, JPCM **26** (2014) 375701;
X. Yi *et al*., EPL, **110** (2015) 36001; J. Marian *et al*., Nuclear Fusion **57** (2017) 092008

Defect production in tungsten

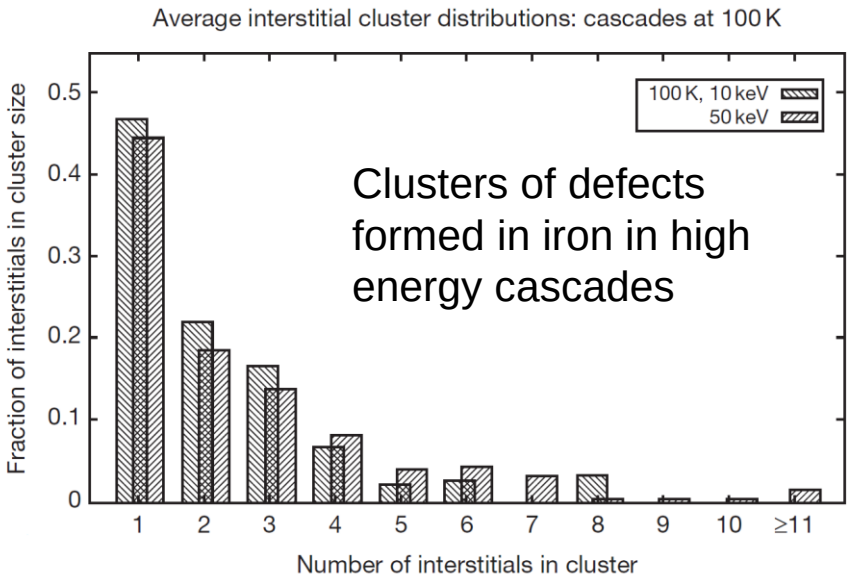

R.E. Stoller (2012) in: Comprehensive Nuclear Materials

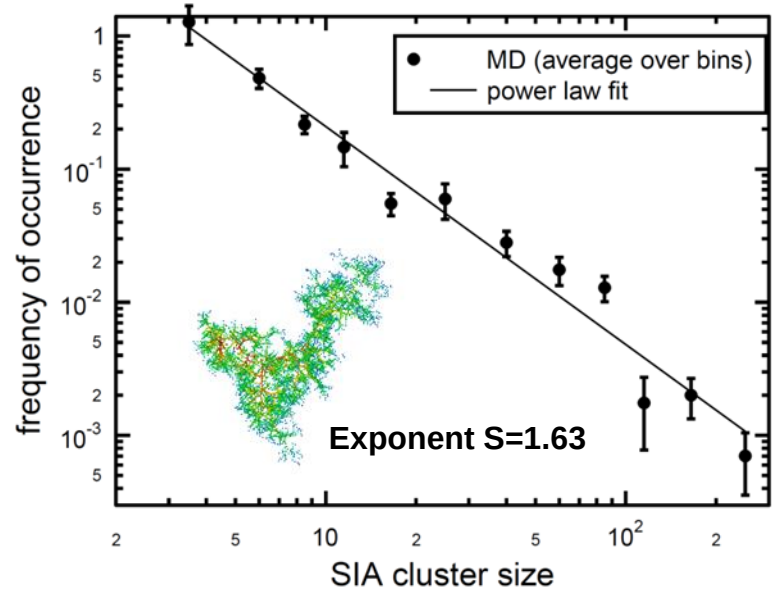

Prior to 1991 it was assumed that defects were produced as Frenkel pairs (individual vacancies and self-interstitials). C.H. Woo and B.N. Singh (1991) noted that clustering of defects in collision cascades may have a significant effect on the evolution of radiation-induced microstructure. Similar findings were reported derived from MD simulations.

T. Diaz de la Rubia, M.W. Guinan, PRL **66** (1991) 2766;
C.H. Woo, B.N. Singh, Phil. Mag. **65** (1992) 889-912

Distribution of defect cluster sizes follows a power law

$$F(n) = \frac{A}{n^S}; n < n^* \approx 600$$

$$A \approx 7.45; S = 1.63$$

A.E. Sand et al., EPL **103** (2013) 46003

Power law of defect clustering

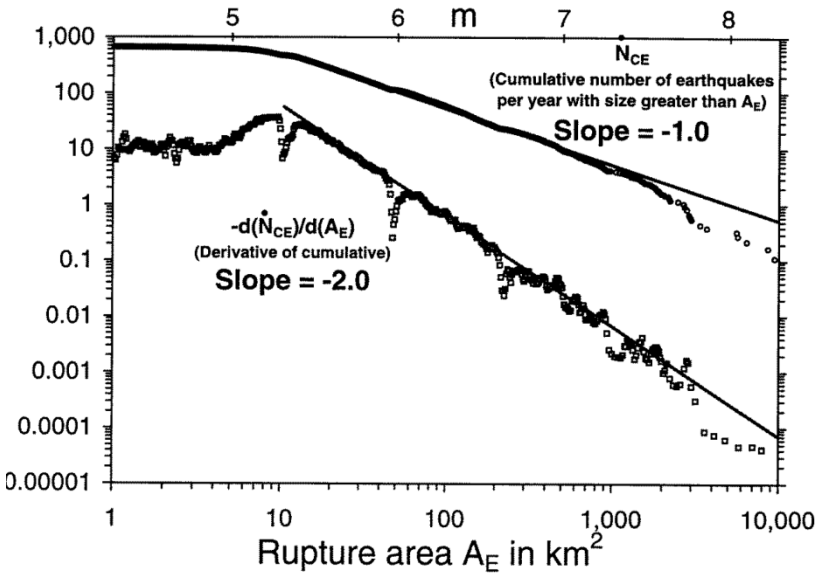

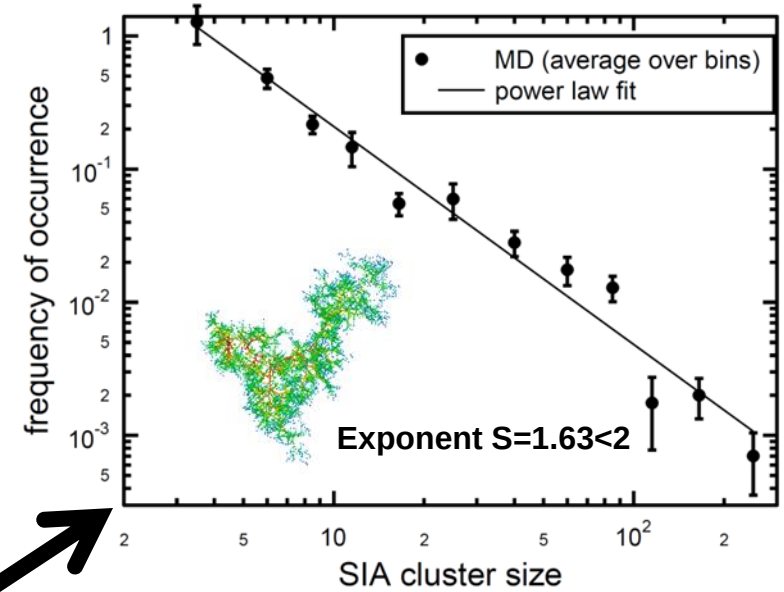

Total number of defects produced

$$N = \sum_{n=1}^{n^*} nF(n) \approx \frac{A}{2-S}(n^*)^{2-S}$$

Distribution of defect cluster sizes follows a power law

$$F(n) = \frac{A}{n^S}; n < n^* \approx 600$$

$$A \approx 7.45; S = 1.63 < 2$$

Large clusters are rare BUT once they form they contain the majority of defects. Large-scale rare events dominate microstructural evolution.

A.E. Sand et al., EPL **103** (2013) 46003

Temperature dependence of defect production

Size distribution of defects in tungsten: 0.01dpa,
From room temperature to 800°C

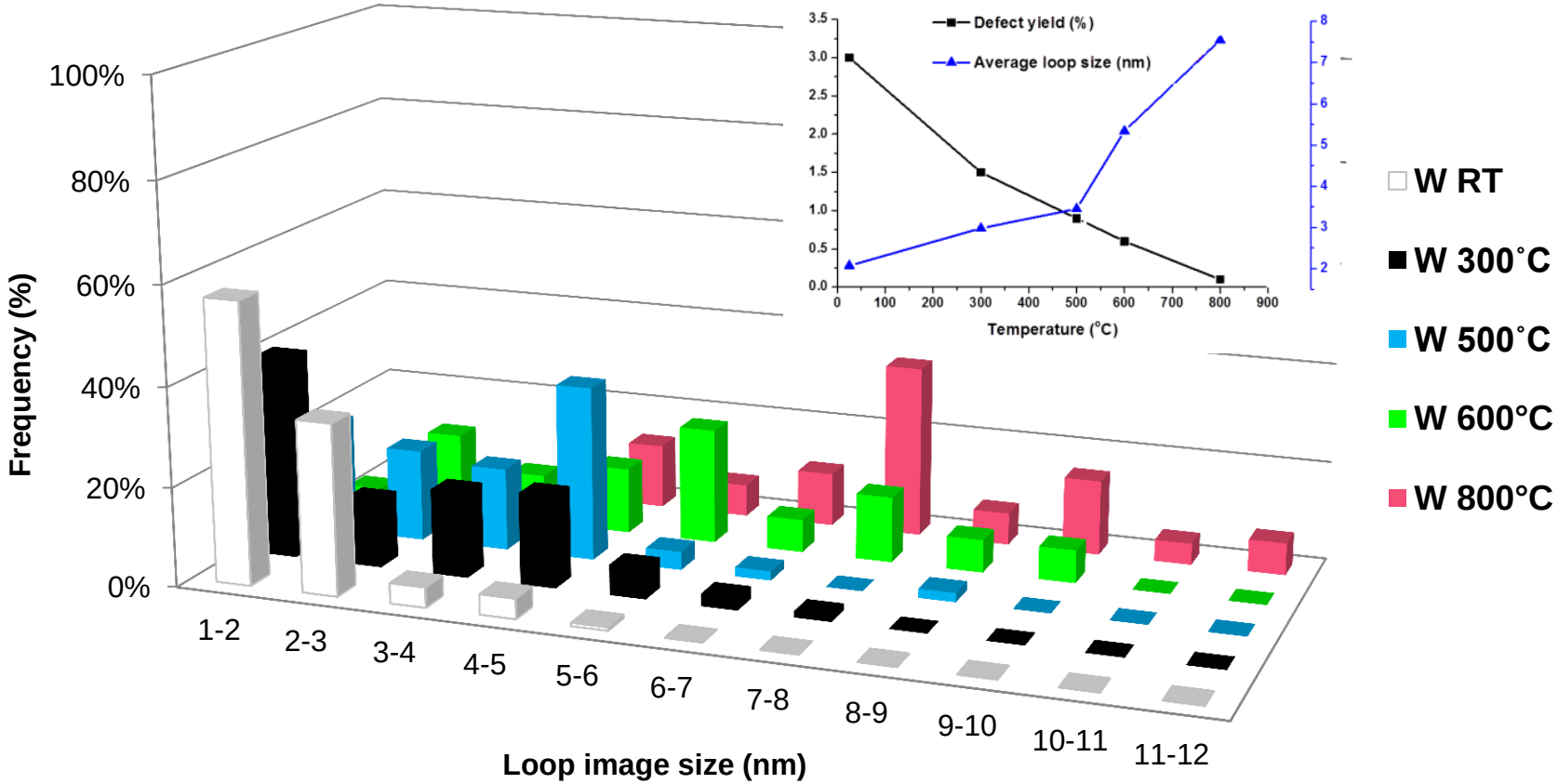

D.R. Mason *et al.*, JPCM **26** (2014) 375701

X. Yi, M.A. Kirk *et al.* In situ ion irradiation experiments performed at Argonne National Laboratory in 2012.

United Kingdom Atomic Energy Authority

CCFE is the fusion research arm of the **United Kingdom Atomic Energy Authority**

CCFE CULHAM CENTRE FOR FUSION ENERGY

Comparison to experiment: loop sizes

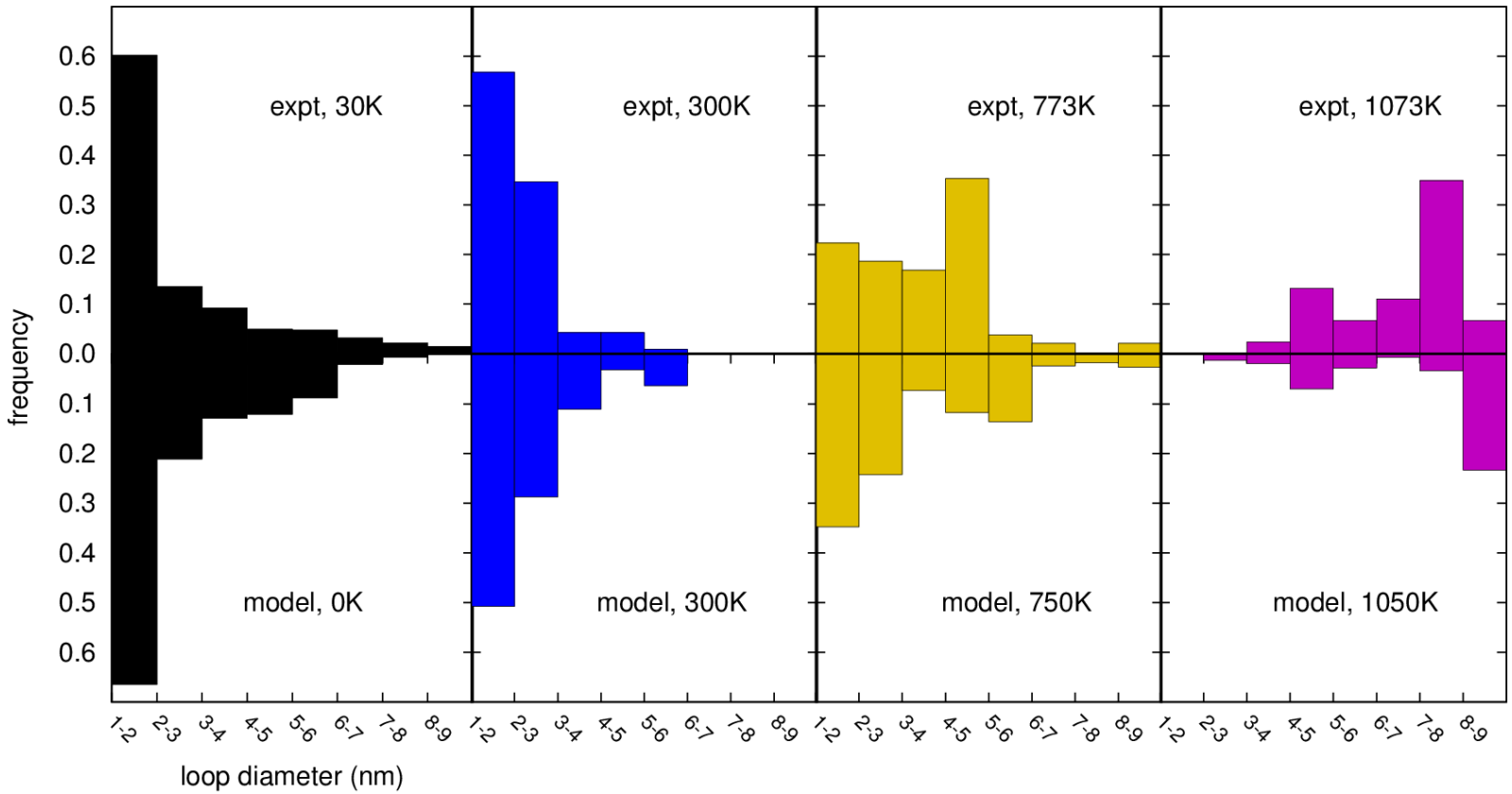

Explaining experimental observations require taking into account interaction between the defects. Fewer but larger defects remain in the material at higher temperatures. Experimental data correspond to the low dose limit (0.01 dpa) where cascades do not overlap. Simulated distributions correspond to t=1 s.

D.R. Mason *et al.*, JPCM **26** (2014) 375701; J. Marian *et al.*, Nuclear Fusion **57** (2017) 092008

A 150 keV cascade in tungsten,
Derlet - Nguyen-Manh - Dudarev
interatomic potential

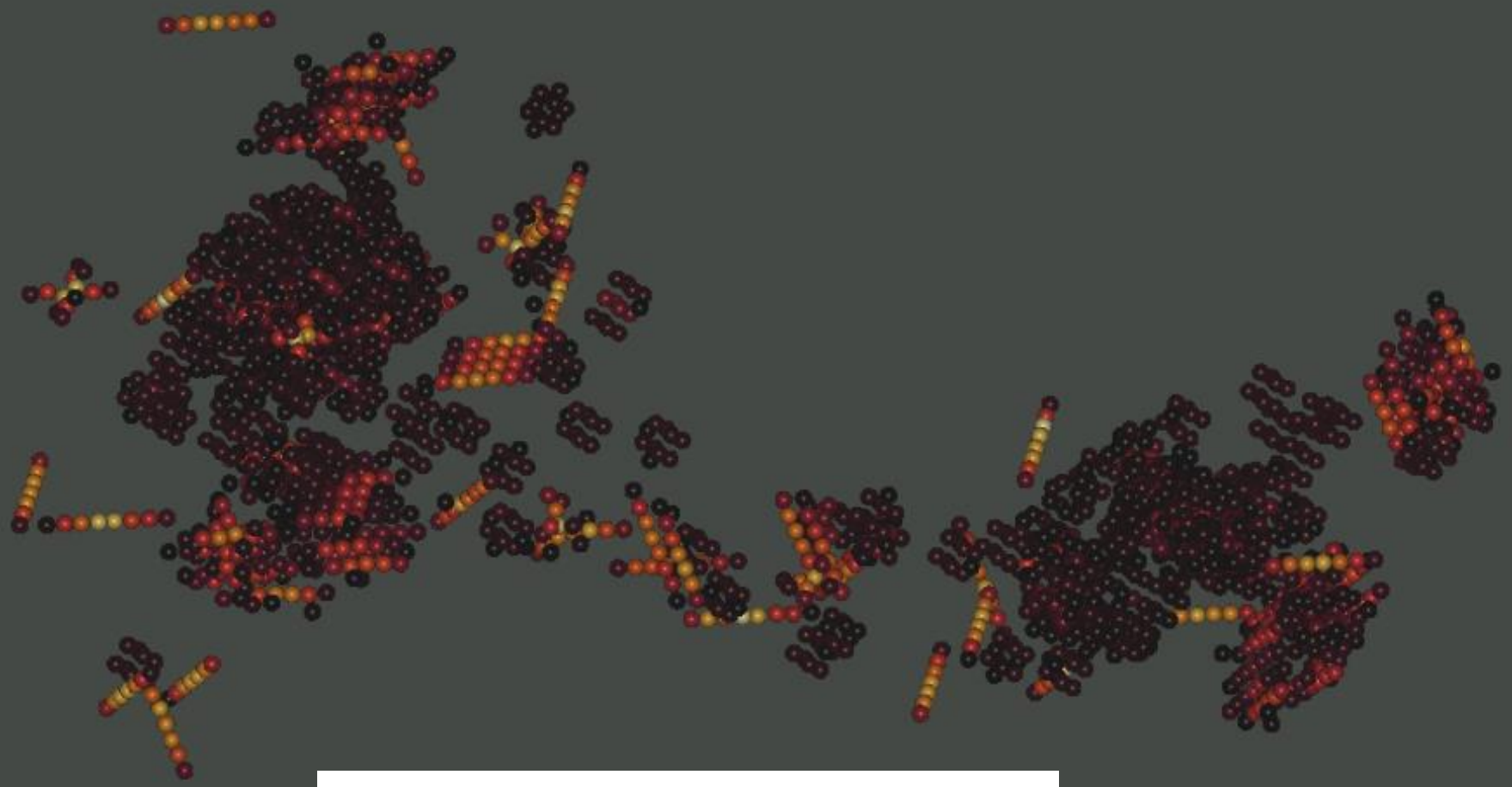

Modelling the evolution of complex cascade configurations still remains one of the most challenging topics in the treatment of radiation damage phenomena.

A 150 keV cascade configuration, courtesy of A.E. Sand

Diffusion of defects: vacancies

	Al	Cu	Au	Ni	Pd	Pt	Pu
E_f	0.580[i]	1.04[d]	0.782[i]	1.37,[e] 1.43,[r] 1.65[r]	1.70[j]	1.18[j]	1.31, 1.36, 1.08[t]
E_m	0.57[m]	0.72[d]	–	1.285,[e] 1.08[r]	–	1.51[j]	–
	V	**Nb**	**Ta**	**Cr**	**Mo**	**W**	**Fe**
E_f	2.51[l]	2.99[l]	3.14[l]	2.64[l]	2.96,[j] 2.96[l]	3.56[l]	2.02,[b] 2.07,[k] 2.15[l]
E_m	0.62[l]	0.91[l]	1.48[l]	0.91[l]	1.28[l]	1.78[l]	0.65,[b] 0.67,[k] 0.64[l]
	C	**Si**	**Ge**	**Be**	**Ti**	**Zr**	**Hf**
E_f	8.2[f]	3.17,[c] 3.29[g]	2.3[h]	0.81,[n] 1.09[o]	1.97,[p] 2.13[q]	2.17,[q] 1.86[s]	2.22[q]
E_m	1.7[f]	0.4[g]	–	0.72B, 0.89NB[o]	0.47B, 0.61NB[p]	0.51B, 0.67NB[q]	0.79B, 0.91NB[q]

It is possible, by means of a DFT calculation, to accurately predict vacancy migration and formation energies in a variety of materials, even where there are no experimental data available. Values derived from DFT calculations are free from impurity effects. It is possible to determine the strength of interaction between vacancies and impurities, also by means of a DFT calculation.

United Kingdom Atomic Energy Authority

Annual Review of Materials Research **43** (2013) 35-61

CCFE is the fusion research arm of the **United Kingdom Atomic Energy Authority**

CCFE CULHAM CENTRE FOR FUSION ENERGY

Diffusion of defects: self-interstitials

	⟨111⟩	⟨110⟩	⟨100⟩	Tetrahedral	Octahedral	E_m
Fe	4.66,[b] 4.45[c]	3.94,[b] 3.75[c]	5.04,[b] 4.75[c]	4.26[c]	4.94[c]	0.34[c]
V	3.37,[d] 3.14[e]	3.65,[d] 3.48[e]	3.92,[d] 3.57[e]	3.84,[d] 3.69[e]	3.96,[d] 3.62[e]	
Nb	5.25[d]	5.60[d]	5.95[d]	5.76[d]	6.06[d]	
Ta	5.83[d]	6.38[d]	7.00[d]	6.77[d]	7.10[d]	
Cr	5.66[d]	5.68[d]	6.64[d]	6.19[d]	6.72[d]	
Mo	7.42,[d] 7.34[e]	7.58,[d] 7.51[e]	9.00,[d] 8.77[e]	8.40,[d] 8.20[e]	9.07,[d] 8.86[e]	
W	9.55[d]	9.84[d]	11.49[d]	11.05[d]	11.68[d]	
Al	1.959[f]	1.869[f]	1.579[f]	1.790[f]	1.978[f]	0.084[f]
Ni	4.69[g]	4.99[g]	4.07[g]	4.69[g]	4.25[g]	0.14[g]
Si	3.84[h]	3.80 (hexagonal)	3.85 (caged)	4.07[h]	4.8	0.18[h]

DFT calculations prove particularly useful in the treatment of self-interstitial atom (SIA) defects. The formation energies of SIA defects are much larger than the formation energies of vacancies, and SIAs do not form thermally at temperatures below 1000ºC. SIAs do form under irradiation (a Frenkel pair = a vacancy + a SIA), making DFT an essential tool for modelling radiation damage phenomena. Values in blue boxes refer to the lowest energy most stable configurations.

United Kingdom Atomic Energy Authority

Annual Review of Materials Research **43** (2013) 35-61

CCFE is the fusion research arm of the **United Kingdom Atomic Energy Authority**

CCFE CULHAM CENTRE FOR FUSION ENERGY

Diffusion of self-interstitial defects in tungsten.

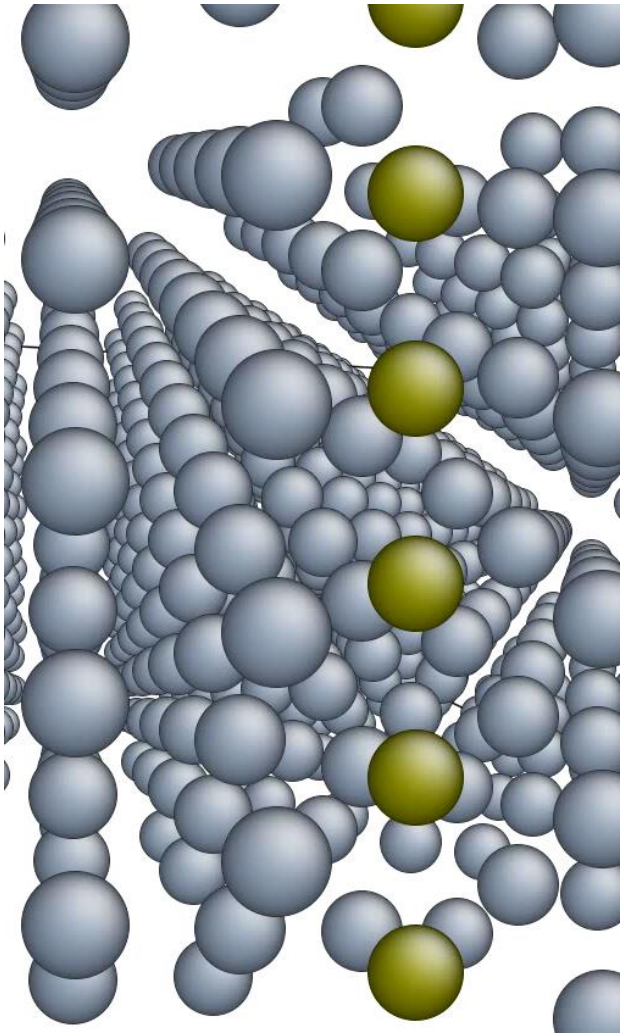

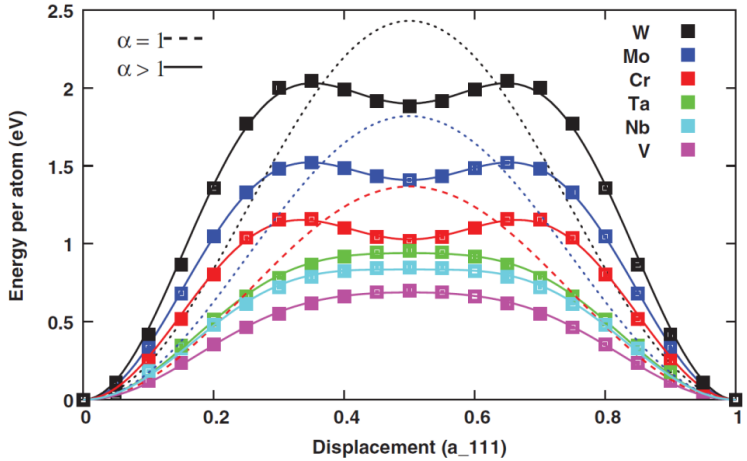

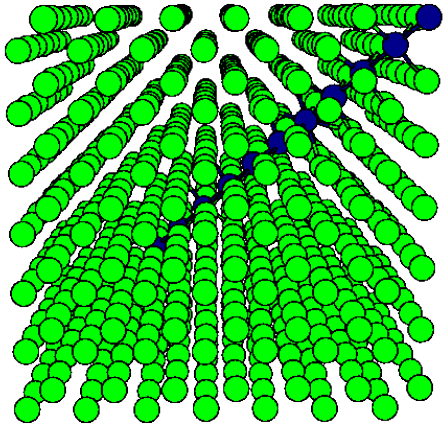

TABLE I. Fitted parameters and derived quantities for the metals of groups V and VI. Also given are the estimated migration temperatures T_m in kelvin, and their experimental values taken from Ref. [2].

Metal	V_0 (eV)	β (eV/a^2)	α	μ	T_m est.	T_m [2]
V	0.689	41.1	1.31	0.575	~8	<6
Nb	0.835	69.1	1.41	0.488	~0.3	<6
Ta	0.940	81.6	1.36	0.477	~0.1	<6
Cr	1.03	63.1	1.73	0.568	~100	~40
Mo	1.41	130	1.66	0.463	~30	35
W	1.90	177	1.64	0.460	~30	27

S.P. Fitzgerald and D. Nguyen-Manh, PRL **101** (2008) 115504

Potential barrier for migration of self-interstitial defects can be estimated analytically by fitting parameters of the Frenkel-Kontorova model to DFT data.

Diffusion of self-interstitial defects in tungsten.

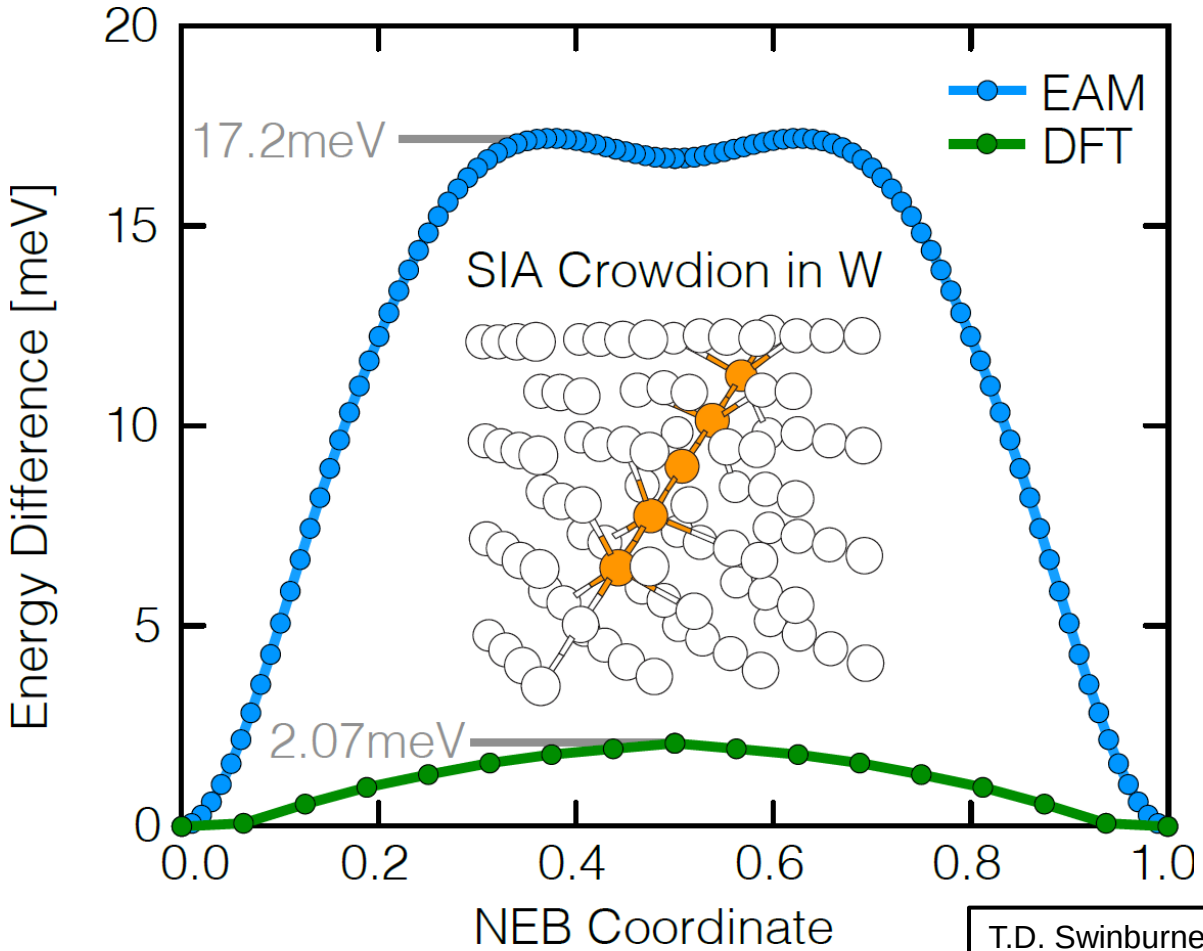

T.D. Swinburne, P.-W. Ma, S.L. Dudarev, New J. Phys. (2017) in press

Interatomic potentials calculations show that the potential barrier for the diffusion of self-interstitial atom defects in tungsten is of the order of 0.017 eV. DFT calculations suggest that the barrier for migration may be even lower, of the order of 0.002 eV. This has implications for diffusion of defects at low temperatures.

Diffusion of defects

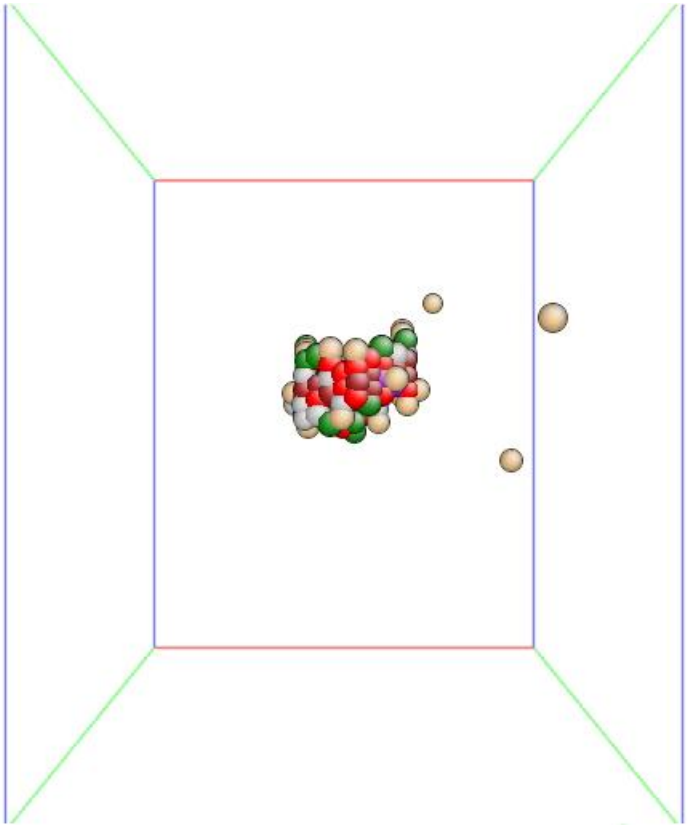

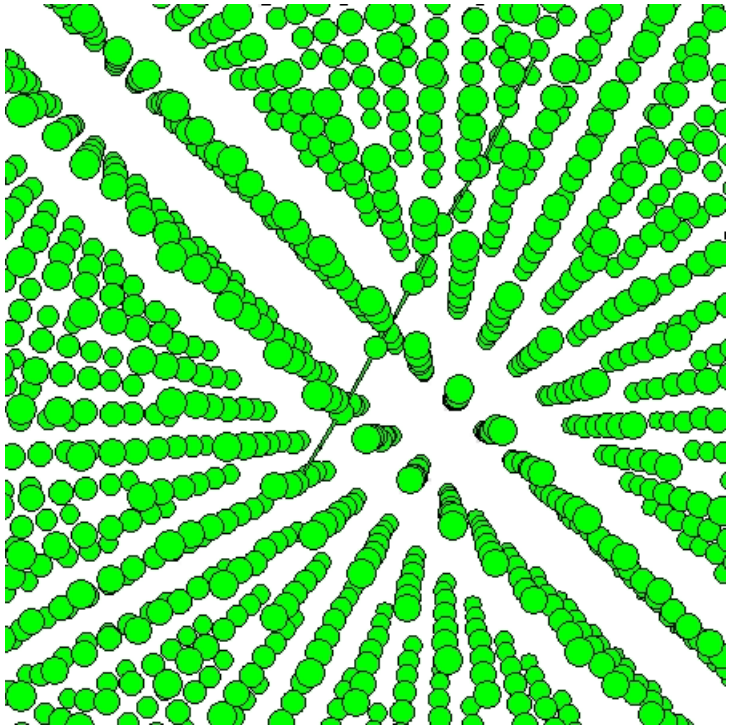

Left: diffusion of a self-interstitial dislocation loop in Fe at 500K, classical molecular dynamics simulations, energy filtering has been applied. Right: diffusion of a single self-interstitial defect in tungsten at 300K, full lattice view.

Diffusion of defects at very low temperatures.

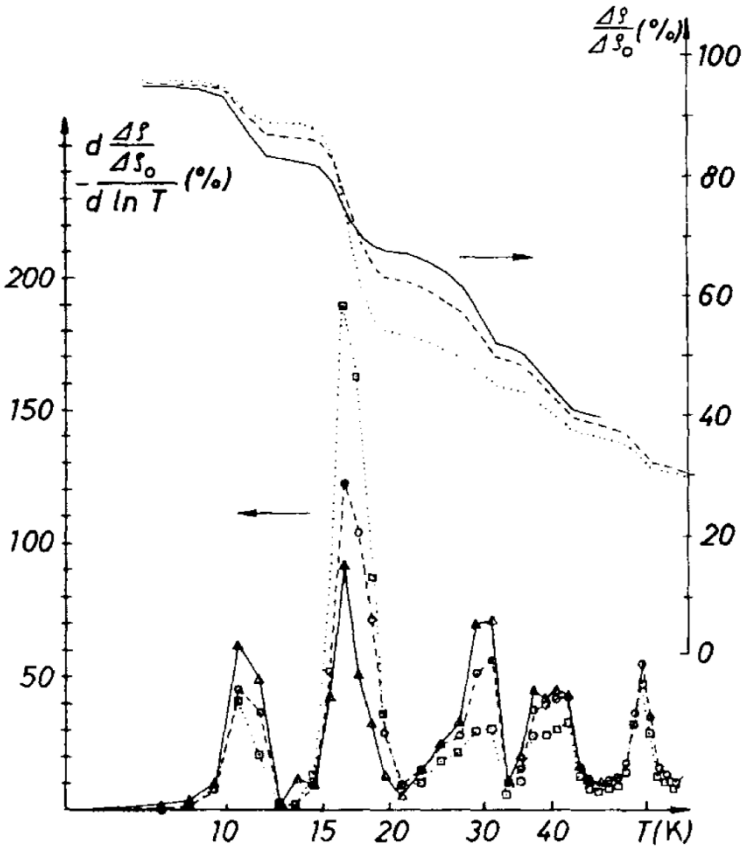

Puzzling low temperature recovery stages in tungsten.

F. Dausinger and H . Schultz, PRL, 35 (1975) 1773,
F. Dausinger, Philos. Magazine A, 37 (1978) 819

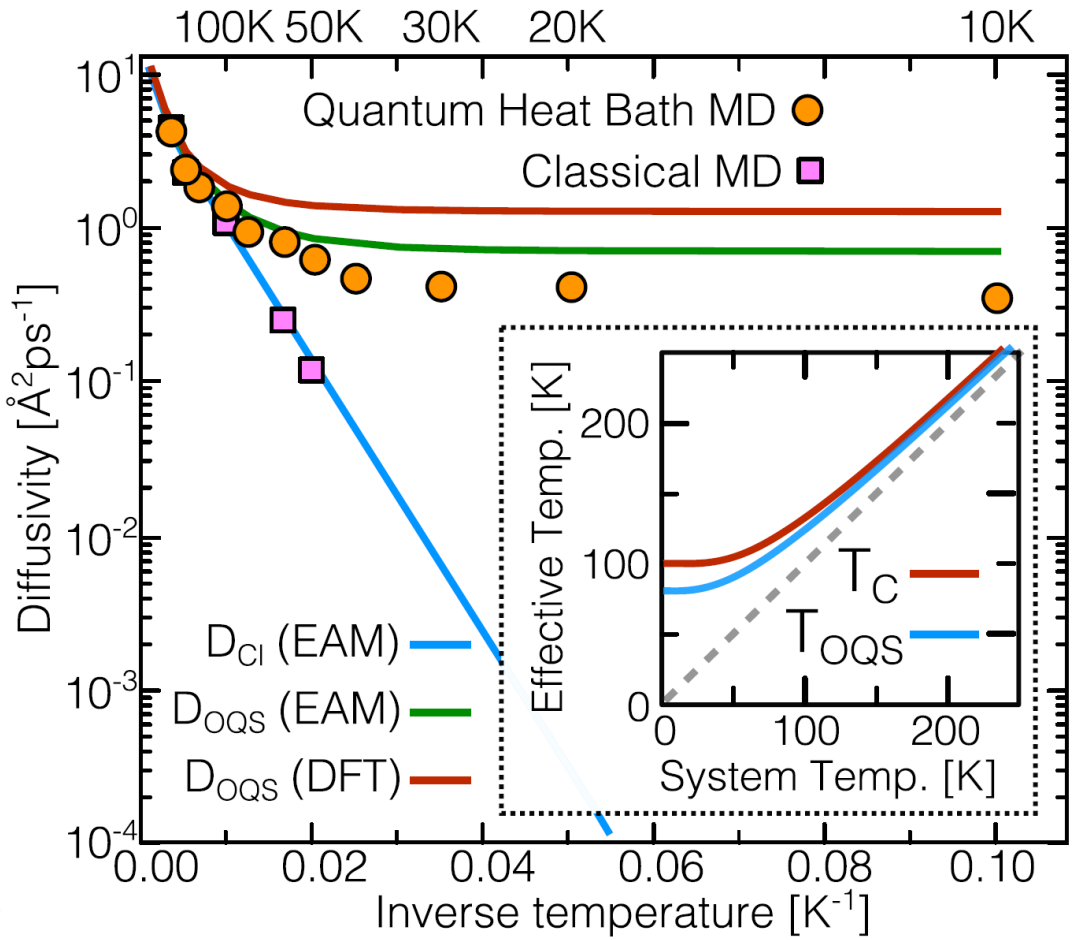

Low temperature diffusivity of self-interstitial defects in tungsten

Thomas D Swinburne[1], Pui-Wai Ma and Sergei L Dudarev

CCFE, UK Atomic Energy Authority, Culham Science Centre, Abingdon, Oxon, OX14 3DB, United Kingdom

[1] Current Address: Theoretical Division T-1, Los Alamos National Laboratory, Los Alamos, NM 87545, United States of America.

New J. Phys. (2017) in press

Diffusion of defects at very low temperatures.

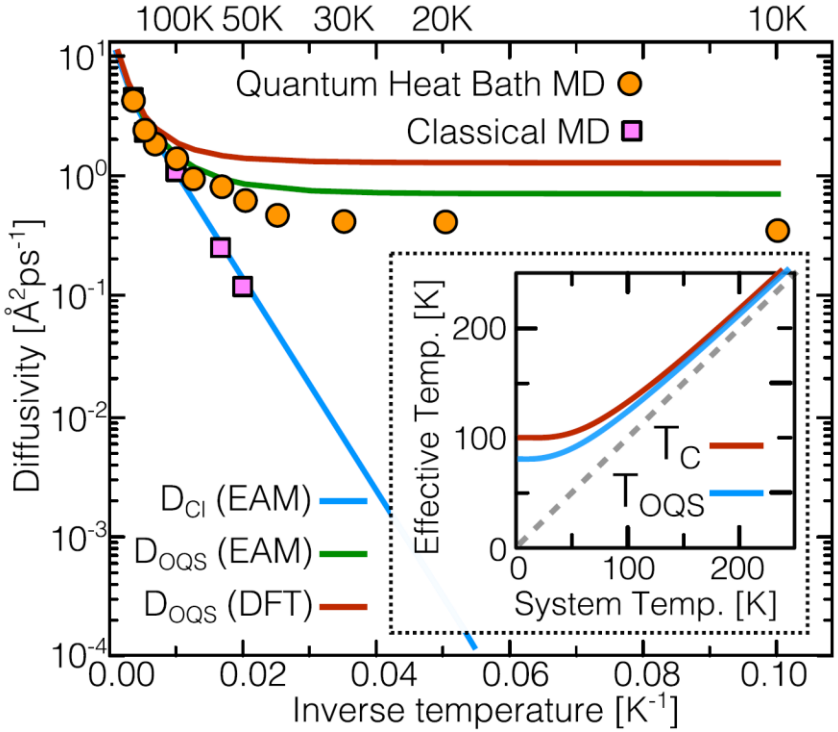

Due to an exceptionally low defect migration barrier, interstitial defects exhibit very high diffusivity of order 10^3 $\mu m^2 s^{-1}$ over the entire range of temperatures from 10 K to 300K.

The origin of high diffusivity is the same as that of zero atomic vibrations, well visible in diffraction experiments as non-zero Debye-Waller factors. No tunnelling is involved, as defects remain heavy classical particles at all temperatures above 1K.

Dislocations: evolution of radiation damage

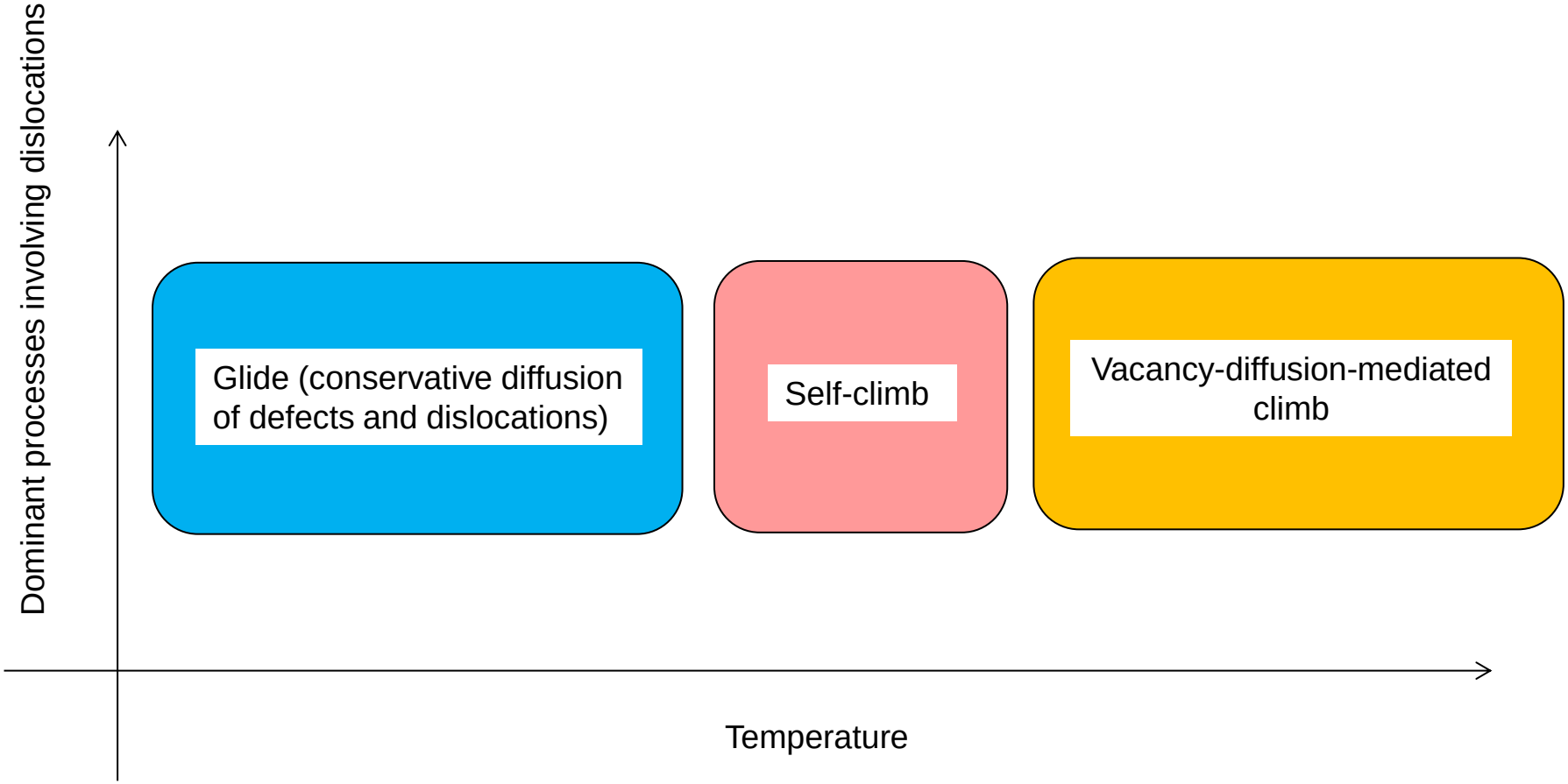

Self-climb of dislocations

The Coalescence of Dislocation Loops by Self Climb

By J. A. Turnbull

Central Electricity Generating Board, Berkeley Nuclear Laboratories,
Berkeley, Gloucestershire GL13 9PB

[Received 15 September 1969]

$$V = -\frac{2\nu a^5 \exp(-E_{sc}/k_B T)}{\pi (k_B T) R^3} \frac{dE}{dx}$$

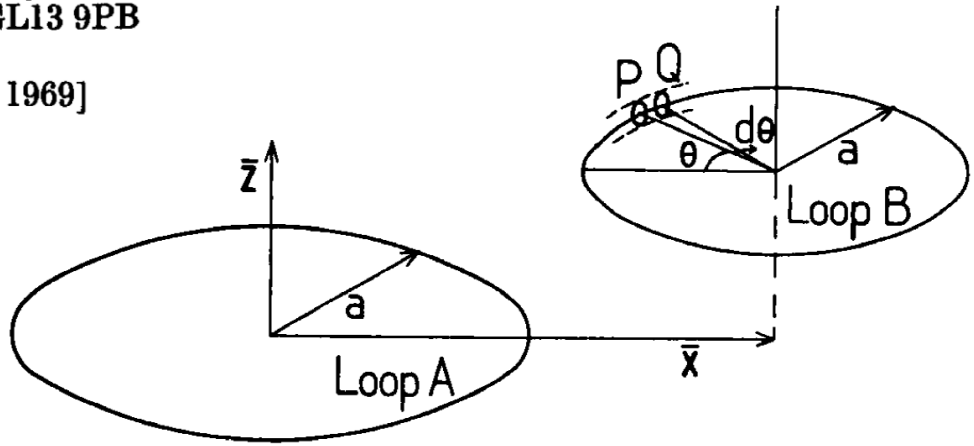

Illustration of the geometry used in § 3.3 when considering the vacancy flux in the segment of pipe PQ on loop B.

Turnbull (1970) showed that interacting dislocation loops coalesce as a result of migration, at loop perimeters, of virtual vacancy-interstitial pairs formed due to thermal fluctuations. No real defects are formed in this process. Loops drift towards each other in the negative direction of gradient dE/dx of elastic interaction energy.

Self-climb of dislocations

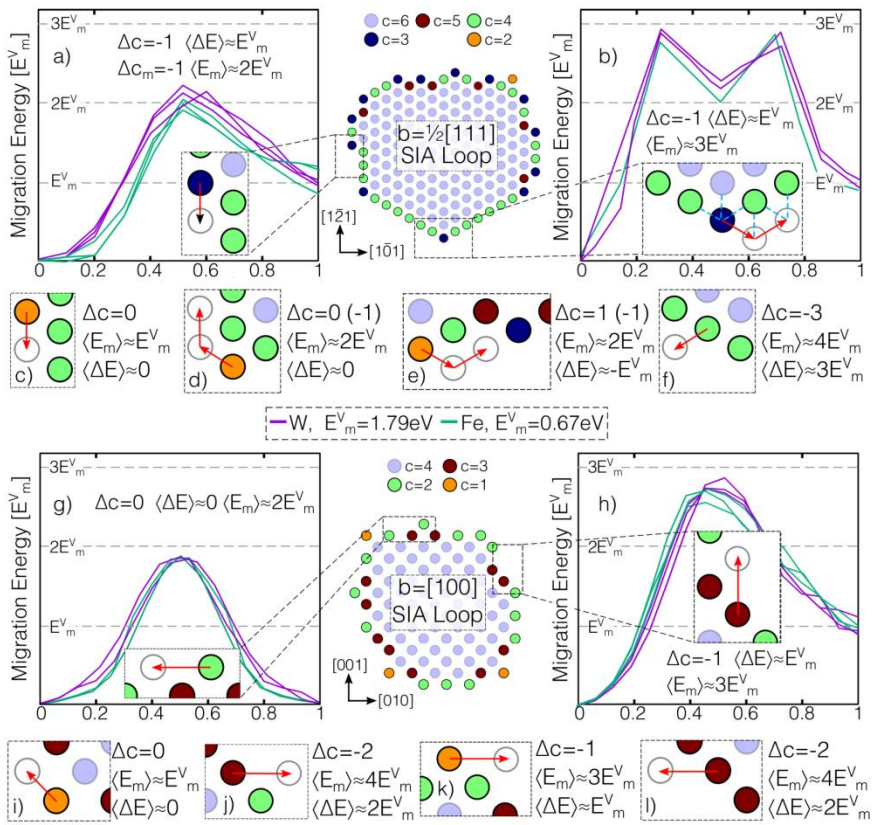

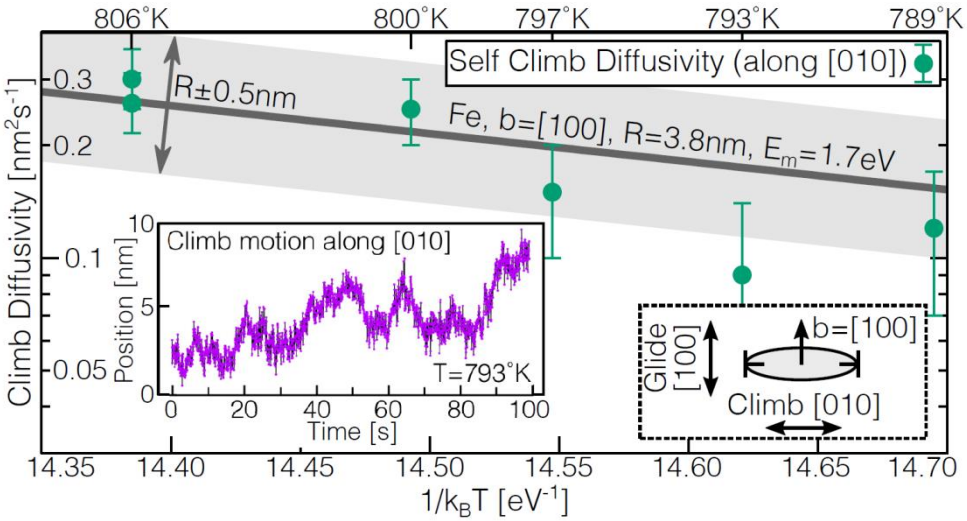

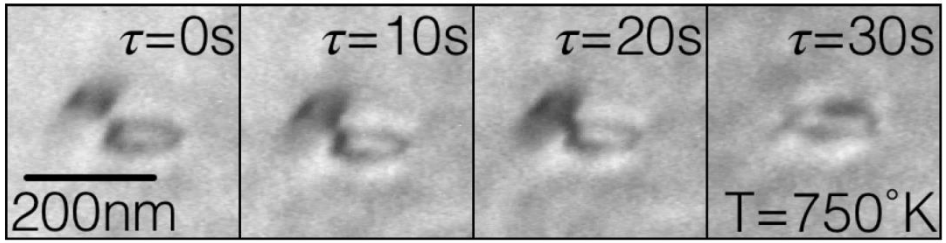

	R_1[nm]	R_2[nm]	d[nm]	T[K]	τ_{exp}[s]	τ_{SC}[s]	τ_{VMC}[s]
Fe	150	30	70	750	30.0	50.2	3.3×10^7
Fe	3.5	3.5	7	660	~0.8	1.8	2.7×10^7
Fe§	~5.	~5.	~10.	725	~6.	2.1	2.7×10^7
W†	20	20	100	1173	66.5	96.2	2.6×10^7
W†	100	500*	100	1273	7.	8.6	1.5×10^5

Dislocation self-climb occurs due to diffusion around the perimeter of dislocation loops, independent of the vacancy atmosphere. At relatively low temperatures this vacancy-free climb is much faster than conventional vacancy-diffusion-mediated climb.

Atomic Energy Authority

CCFE is

T.D. Swinburne *et al.*, Sci Repts. 6 (2016) 30596

rity

CULHAM CENTRE FOR FUSION ENERGY

Real space models for microstructure

Three-dimensional formulation of dislocation climb

Yejun Gu [a], Yang Xiang [b,*], Siu Sin Quek [c], David J. Srolovitz [d,e]

Journal of the Mechanics and Physics of Solids 83 (2015) 319–337

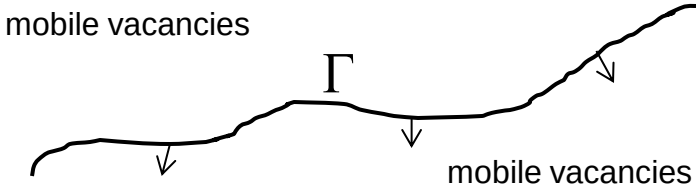

$$\frac{\partial c(\mathbf{x},t)}{\partial t} = -\Omega \nabla J(\mathbf{x},t) - \Omega I(\mathbf{x},t)\delta(\Gamma)$$

$$J(\mathbf{x},t) = -\frac{D_v c(\mathbf{x},t)}{\Omega k_B T}\nabla \mu_v(\mathbf{x},t)$$

Here Γ defines a dislocation line, so that $\int \delta[\Gamma] f(\mathbf{x}) d^3x = \int_\Gamma f(\mathbf{x}) ds.$

In the dilute gas approximation for the chemical potential of vacancies, we arrive at the boundary value problem for a moving dislocation line. A dislocation line moves due to elastic forces acting on it, which stimulate absorption or emission of vacancies:

$$\mu_v(\mathbf{x},t) = k_B T \ln c(\mathbf{x},t);$$

$$D_v \nabla^2 c = b_e v_{cl} \delta(\Gamma)$$

$$c(|\mathbf{x}| \to \infty) = c_\infty$$

Real space models for microstructure

Three-dimensional formulation of dislocation climb

Yejun Gu [a], Yang Xiang [b,*], Siu Sin Quek [c], David J. Srolovitz [d,e]

Journal of the Mechanics and Physics of Solids 83 (2015) 319–337

The central step is the conversion of the boundary value problem into an integral equation

$$c(\mathbf{x}) = \frac{1}{4\pi D_v} \oint_\Gamma \frac{\mathbf{b}\cdot(\mathbf{v}\times d\,\mathbf{l}')}{|\mathbf{x}-\mathbf{x}'|} + c_\infty .$$

Assume that a dislocation line forms a closed loop. At large distances from the loop, where |**x**-**x**'|>> loop size, this equation acquires a simple form:

$$c(\mathbf{x}) \approx \frac{1}{4\pi D_v |\mathbf{x}|} \oint_\Gamma \mathbf{b}\cdot(\mathbf{v}\times d\,\mathbf{l}') + c_\infty .$$

Here

$\oint_\Gamma \mathbf{b}\cdot(\mathbf{v}\times d\,\mathbf{l}') = \frac{d\Omega_{rel}}{dt}$, and $\Omega_{rel}(t)$ is the <u>volume</u> of the dislocation loop.

Relaxation volume of a dislocation loop

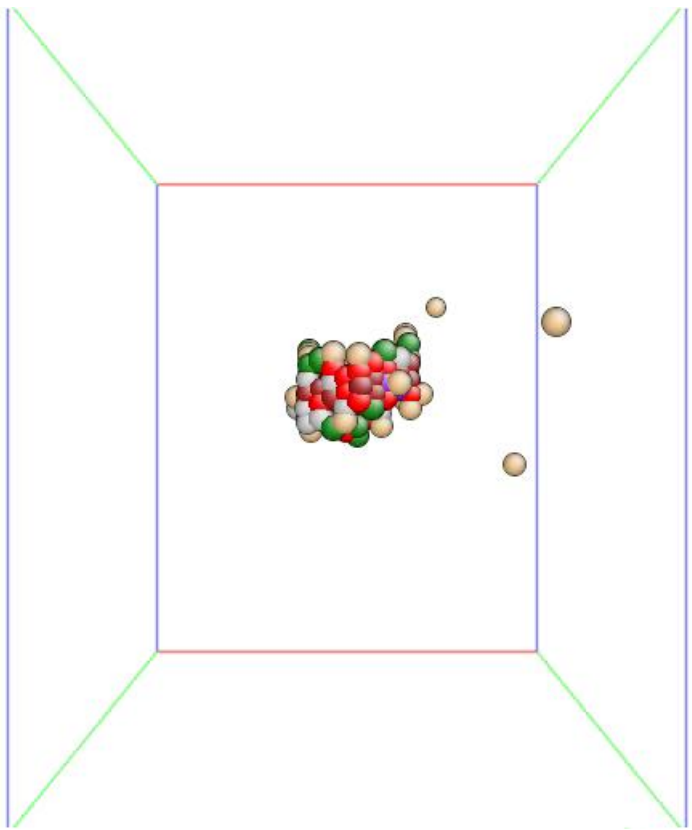

Molecular dynamics simulation of thermal Brownian motion of a ½(111) dislocation loop in iron at 500K.

Formula for the relaxation volume of a dislocation loop

$$\Omega_{rel}(t) = (\mathbf{b} \cdot \mathbf{A}(t))$$

shows that the volume of a loop remains constant even though the direction and magnitude of the loop vector area changes. Left: simulation of Brownian motion of a dislocation loop in Fe. Below: experimental observation of Brownian motion of a dislocation loop, courtesy of Prof. K. Arakawa.

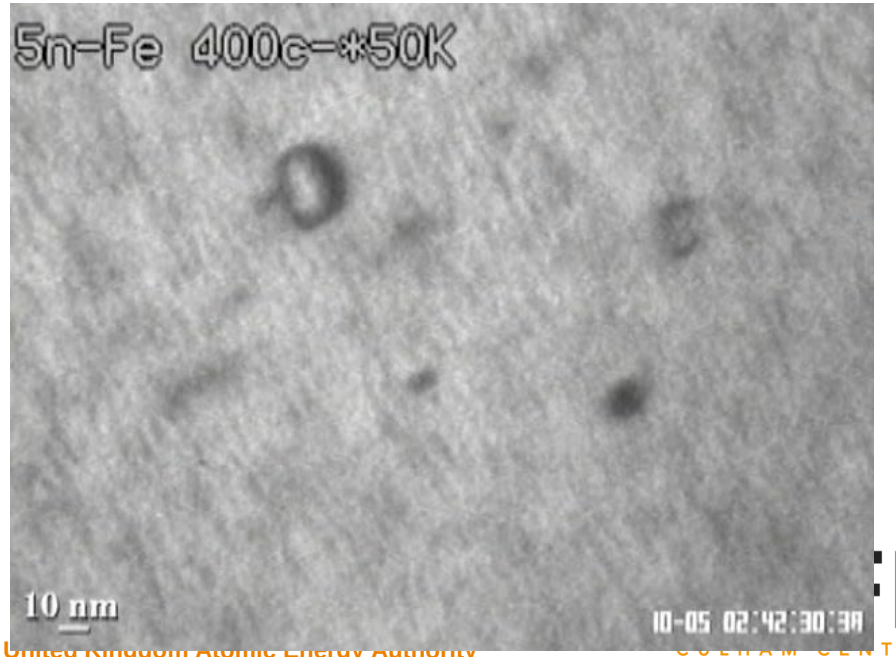

$$\boxed{\frac{d\Omega_{rel}}{dt} = \frac{d}{dt}(\mathbf{b} \cdot \mathbf{A}(t)) = 0.}$$

United Kingdom Atomic Energy Authority

CCFE CULHAM CENTRE FOR FUSION ENERGY

Real space models for microstructure

The field of vacancies changes adiabatically, following the evolution of dislocation loops (centres of loops are at $\mathbf{x}_i$)

$$c(\mathbf{x}) \approx c_\infty + \frac{1}{4\pi D_v} \sum_i \frac{1}{|\mathbf{x}-\mathbf{x}_i|} \frac{d\Omega_{rel}^i}{dt}.$$

Volume Ω_{rel} of a dislocation loop with Burgers vector $\mathbf{b}$ and area vector $\mathbf{A}$ is given by the scalar product $(\mathbf{b}\cdot\mathbf{A})$. Volume is positive for an interstitial loop and negative for a vacancy loop.

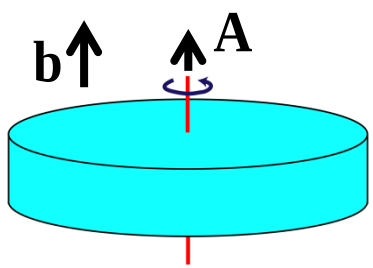

Interstitial loop, $\Omega_{rel} > 0$

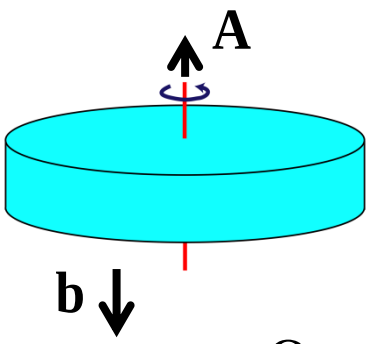

vacancy loop, $\Omega_{rel} < 0$

Above equations for c(**x**) can also be formulated as a set of ODEs for the velocities of nodal points on dislocation lines.

Diffusion to/from surfaces

The computational efficiency of the treatment developed by Y. Gu, Y. Xiang *et al.*, JMPS (2015) is fundamentally due to the use of "free-space" Green's function

$$G_0(\mathbf{x},\mathbf{x}') = -\frac{1}{4\pi D_v\,|\mathbf{x}-\mathbf{x}'|}.$$

This computational advantage is lost if, in order to take into account the boundary conditions, we attempt to modify these Green's functions. An alternative approach is the Kirchhoff integral approximation, which retains the use of <u>free</u> Green's functions

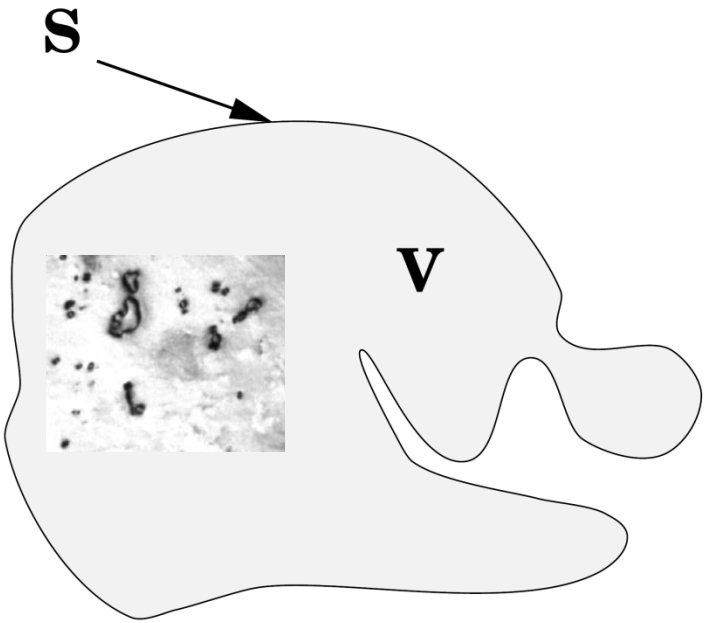

$$\int_V dV\left[\Phi_a(\mathbf{x})\frac{\partial^2\Phi_b(\mathbf{x})}{\partial\mathbf{x}^2} - \Phi_b(\mathbf{x})\frac{\partial^2\Phi_a(\mathbf{x})}{\partial\mathbf{x}^2}\right]$$

$$= \int_S d\mathbf{S}\left[\Phi_a(\mathbf{x})\frac{\partial\Phi_b(\mathbf{x})}{\partial\mathbf{x}} - \Phi_b(\mathbf{x})\frac{\partial\Phi_a(\mathbf{x})}{\partial\mathbf{x}}\right]$$

This formula is known as Green's theorem (G. Green, 1828). It provides the means for treating surfaces and retains the advantages offered by the free Green's function formalism.

Diffusion to/from surfaces

We choose one of the functions in Green's theorem as the vacancy concentration field. The other is free Green's function. This formula below shows that vacancy field can be evaluated everywhere, if c(**x**) and its normal derivatives at surfaces are known.

$$\int_V dV'\left[c(\mathbf{x}')\frac{\partial^2 G_0(\mathbf{x},\mathbf{x}')}{\partial \mathbf{x}'^2} - G_0(\mathbf{x},\mathbf{x}')\frac{\partial^2 c(\mathbf{x}')}{\partial \mathbf{x}'^2}\right] = \int_S dS'\left[c(\mathbf{x}')\left(\mathbf{n}\cdot\frac{\partial G_0(\mathbf{x},\mathbf{x}')}{\partial \mathbf{x}'}\right) - G_0(\mathbf{x},\mathbf{x}')\left(\mathbf{n}\cdot\frac{\partial c(\mathbf{x}')}{\partial \mathbf{x}'}\right)\right]$$

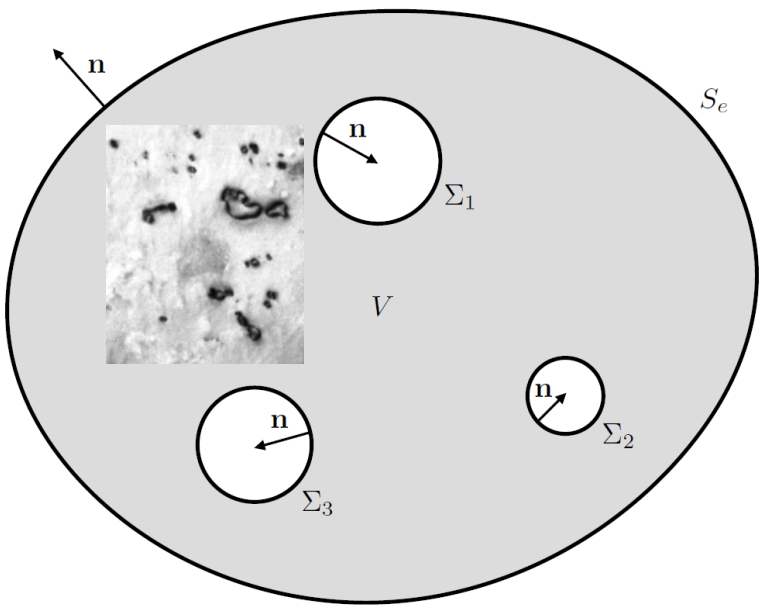

In the right-hand side of this equation, vacancy concentration at a point **x**', situated at a surface, can be evaluated using the same approach as the one developed for the dislocation loops.

Evaporation of vacancies from dislocation loops is driven by elastic self-stress. In the case of surfaces, it is driven by surface tension.

Arrive at a system of coupled ODEs for the velocities of nodes on dislocation lines <u>and</u> at surfaces. This fully defines the dynamics of diffusion-mediated evolution of loops and cavities/surfaces.

United Kingdom Atomic Energy Authority

Journal of the Mechanics and Physics of Solids 103 (2017) 121–141

Diffusion to/from surfaces

Equations, describing the vacancy diffusion-mediated evolution of dislocation loops, cavities *and* the external surface, have the form:

$$\omega(\mathbf{x})c(\mathbf{x}) = D_v \int_S dS' \left[c(\mathbf{x}')\left(\mathbf{n} \cdot \frac{\partial G_0(\mathbf{x},\mathbf{x}')}{\partial \mathbf{x}'} \right) - G_0(\mathbf{x},\mathbf{x}')\left(\mathbf{n} \cdot \frac{\partial c(\mathbf{x}')}{\partial \mathbf{x}'} \right) \right]$$

Here $\omega(\mathbf{x}) = 1$ in the bulk, $\omega(\mathbf{x}) = 1/2$ at surfaces (this comes from the integration of a delta-function at the surface) and $\omega(\mathbf{x}) = 0$ in the vacuum. 'Surfaces' also include the toroidal surfaces wrapped around dislocation lines.

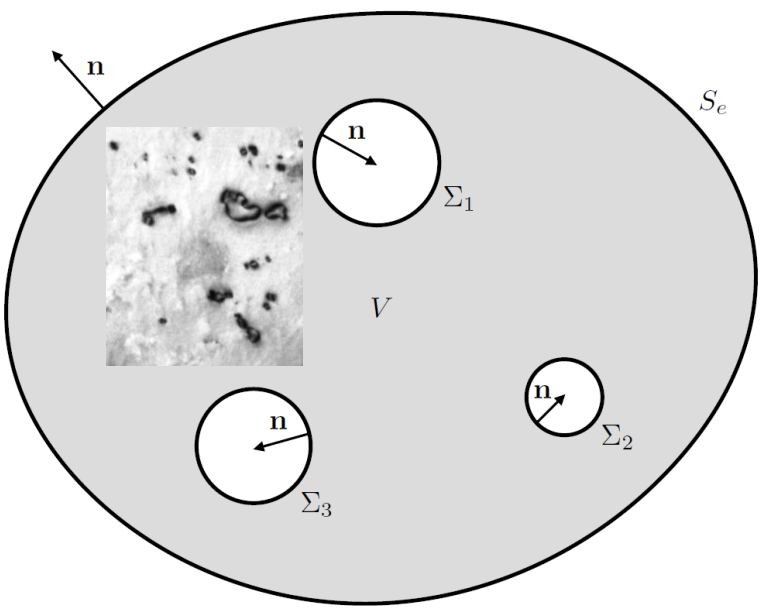

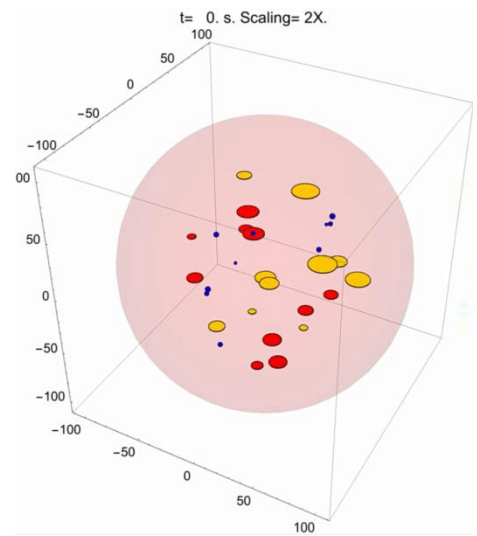

This animation shows evolution of voids, interstitial and vacancy dislocation loops, evolving through the evaporation and exchange of vacancies in tungsten at 1750K.

Applications: evolution timescales

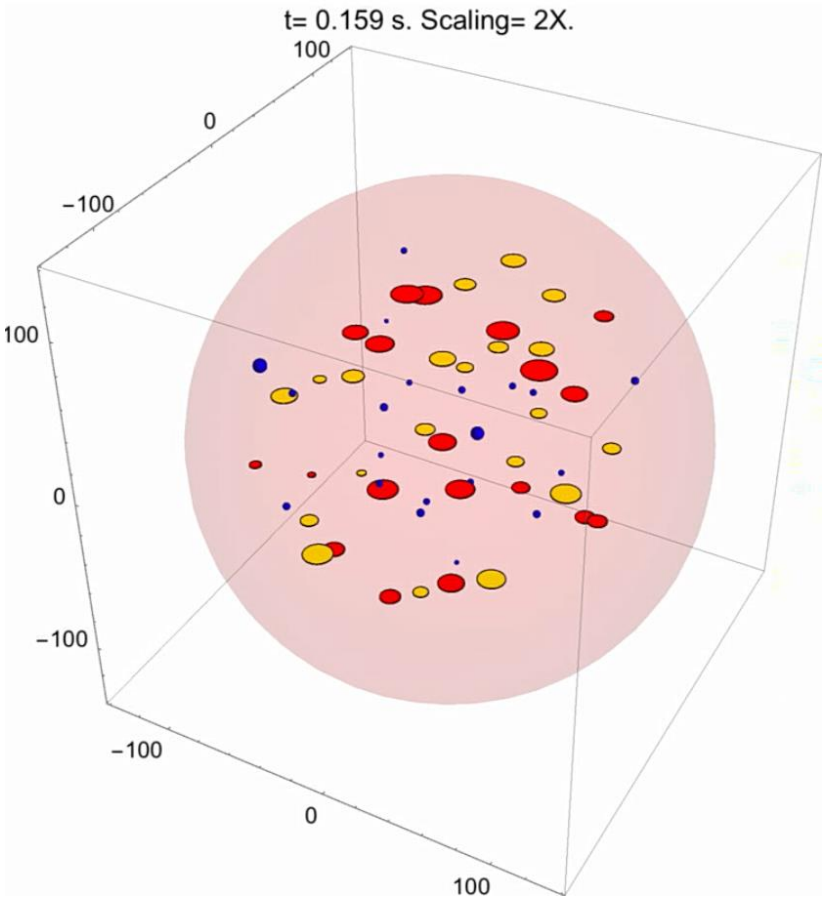

Evolution of 20 cavities, 20 interstitial loops and 20 vacancy loops randomly distributed with the average number density $5x10^{-6}$ nm^{-3}, in a spherical sample of radius R=142 nm. Objects' radii are initially normally distributed: with the mean of 3.2 nm and standard deviation of 1 nm (loops); with the mean of 1 nm and standard deviation of 0.1 nm (18 smaller cavities); with the mean of 2.2 nm and standard deviation of 0.22 nm (for the two larger cavities).

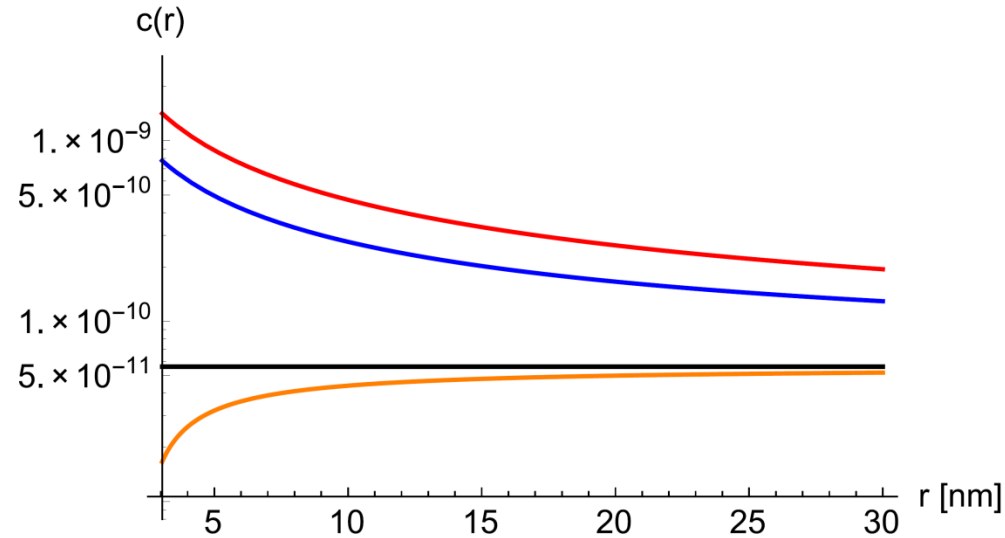

Vacancy concentration profiles found in a typical simulation. Vacancy loops (red) and voids (blue) generate local zones with high concentration of diffusing vacancies, exceeding the background concentration by over two orders of magnitude. Interstitial loops produce local vacancy depleted zones.

Journal of the Mechanics and Physics of Solids 103 (2017) 121–141

Decomposition of W-Re alloys under irradiation

Transmutations due to exposure to fusion neutrons

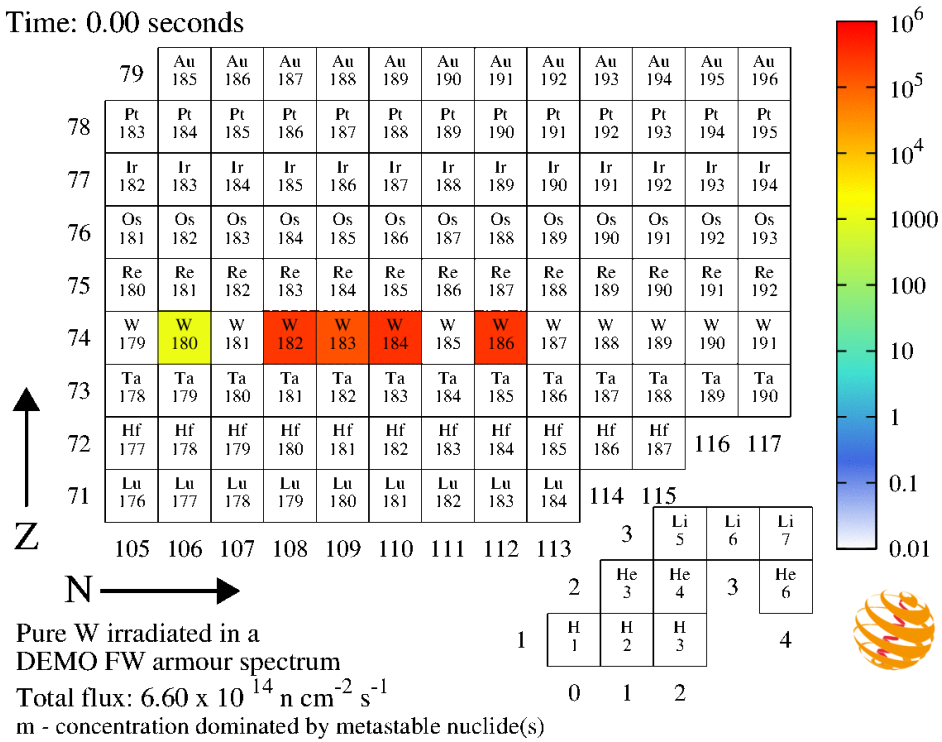

Pure W irradiated in a DEMO FW armour spectrum

Total flux: 6.60 x 10^{14} n cm^{-2} s^{-1}

m - concentration dominated by metastable nuclide(s)

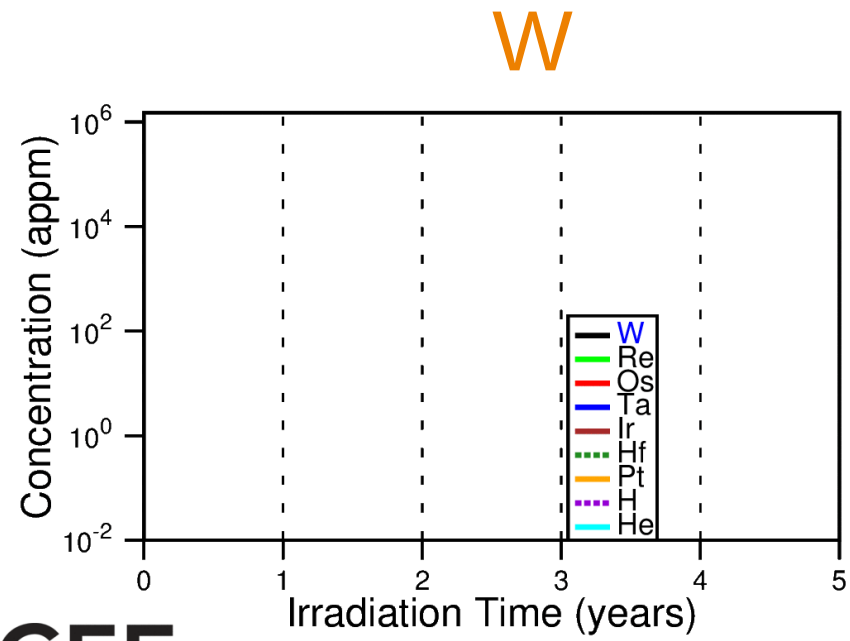

M. R. Gilbert et al., *Nucl. Sci. Eng* (2013)

M.R. Gilbert et al., *Nucl. Fusion* **51** (2011) 043005 & **52** (2012) 083019

Initially pure natural tungsten, exposed to neutrons with the spectrum of a DEMO fusion reactor, transforms into other elements, including rhenium, osmium, helium and hydrogen. Accumulation of rhenium gives rise to the formation of Re-rich precipitates, which embrittle tungsten and reduce its thermal conductivity.

M.R. Gilbert et al., Nucl. Fusion **57** (2017) 044002

Anomalous segregation in W-Re alloys

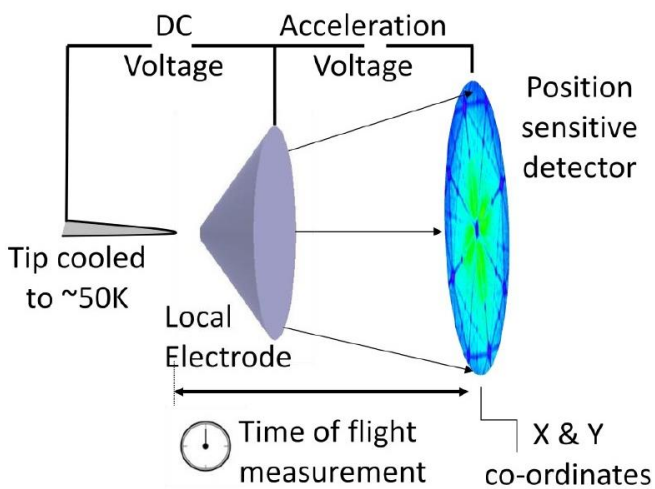

W-2Re

Concentration Map

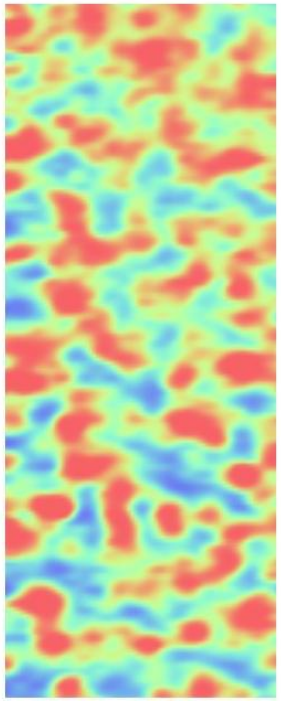

Re Atom Map

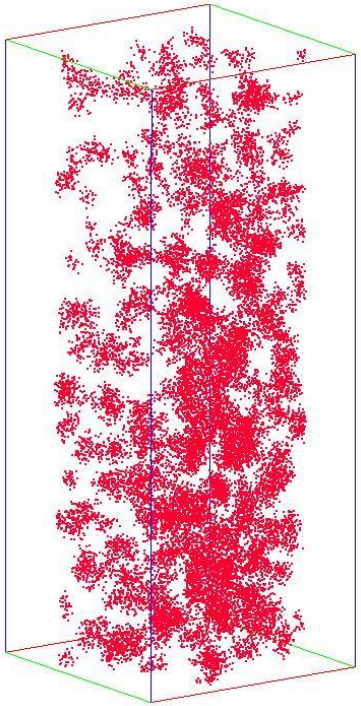

Atom probe observation of segregation of Re in W-2%Re alloy under ion irradiation.

The puzzling aspect of this phenomenon is that under irradiation, rhenium forms precipitates in highly dilute alloys that, according to equilibrium thermodynamics, should exhibit full solubility.

A. Xu *et al.*, *Acta Materialia* **87** (2015) 121

Anomalous segregation in W-Re alloys

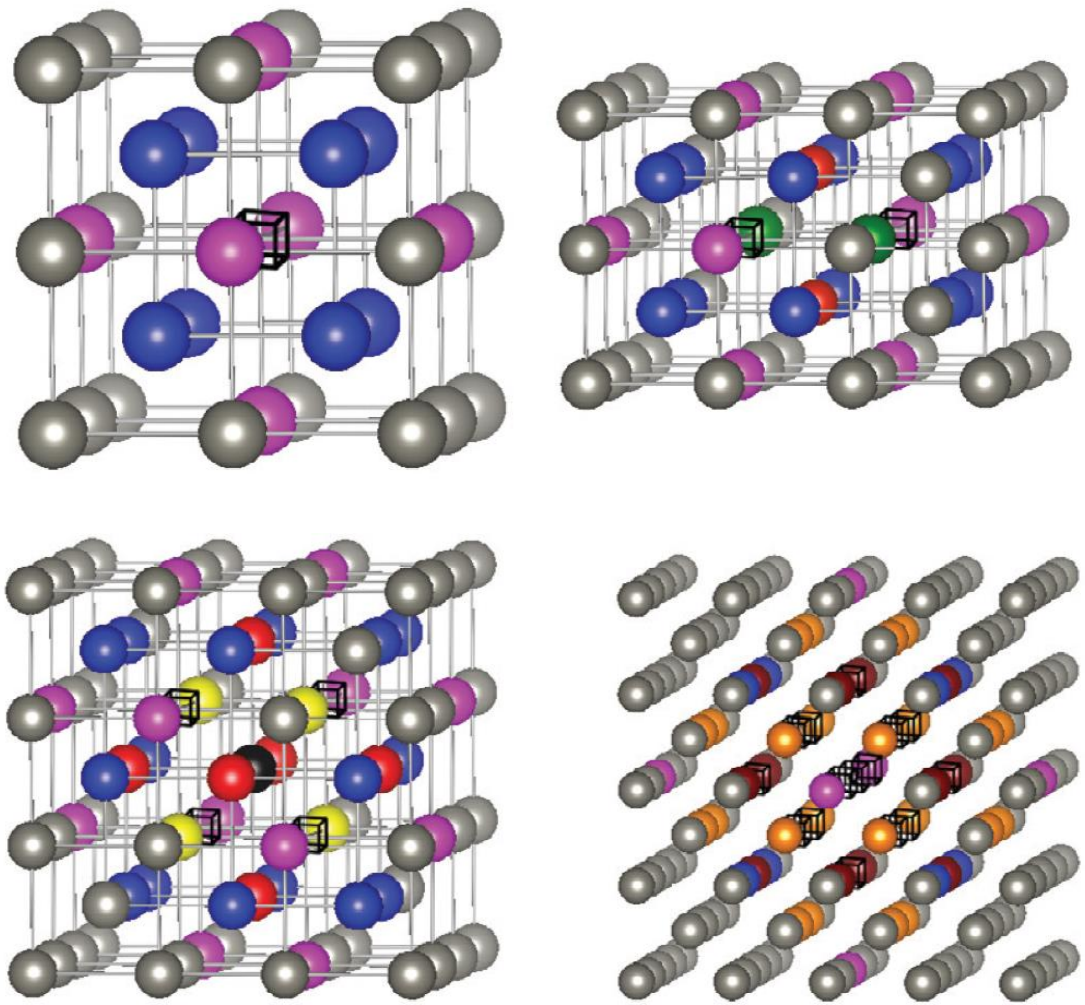

Model for binary W-Re alloys + vacancies as ternary W-Re-vacancy alloys. This is possible because lattice deformations, associated with vacancies, are small.

J. Wrobel *et al.*, J. Phys.: Condens. Matter **29** (2017) 145403

Anomalous segregation in W-Re alloys

J. Phys.: Condens. Matter **29** (2017) 145403 J S Wróbel *et al*

Table 1. Monte Carlo results as functions of Re and vacancy concentration for alloys quenched down from high temperatures. MC simulations were performed starting from 2500 K. Alloys were cooled down with the temperature step of 100 K to the temperature of 100 K with 3000 MC steps per atom performed both at thermalization and accumulation stages.

	1% at. Re	2% at. Re	5% at. Re	10% at. Re
0.05% at. Vac	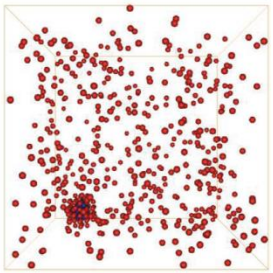	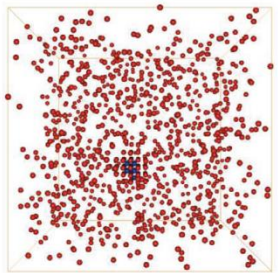	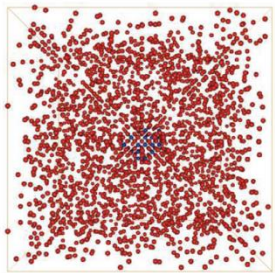	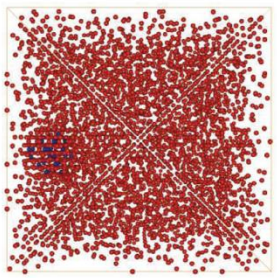
0.1% at. Vac	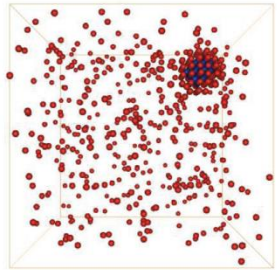	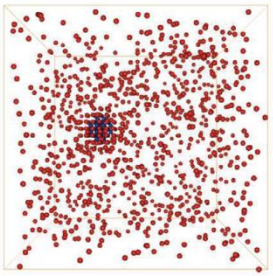	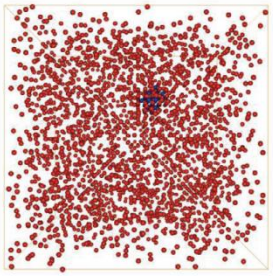	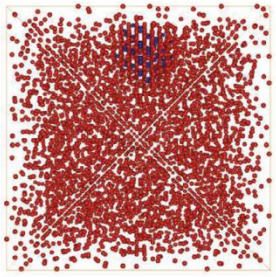
0.2% at. Vac	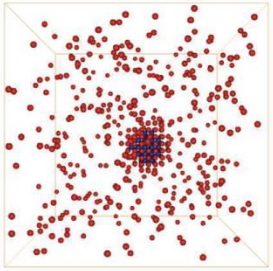	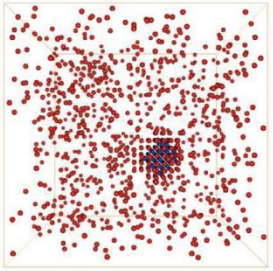	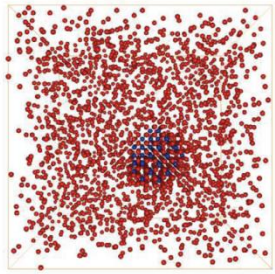	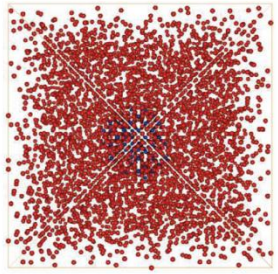

Vacancies act as nucleation centres for rhenium precipitates.

J. Wrobel *et al.*, J. Phys.: Condens. Matter **29** (2017) 145403

IOP Publishing | International Atomic Energy Agency Nuclear Fusion

Nucl. Fusion 57 (2017) 092008 (26pp) https://doi.org/10.1088/1741-4326/aa5e8d

Recent advances in modeling and simulation of the exposure and response of tungsten to fusion energy conditions

Jaime Marian[1,a], Charlotte S. Becquart[2], Christophe Domain[3], Sergei L. Dudarev[4], Mark R. Gilbert[4], Richard J. Kurtz[5], Daniel R. Mason[4], Kai Nordlund[6], Andrea E. Sand[6], Lance L. Snead[7], Tomoaki Suzudo[8] and Brian D. Wirth[9]

[1] University of California Los Angeles, Los Angeles, CA, United States of America
[2] UMET, UMR 8207, ENSCL, U Lille, 59655 Villeneuve d'Ascq Cédex, France
[3] EDF-R&D, Département MMC, Les Renardières, F-77250 Moret sur Loing, France
[4] Culham Centre for Fusion Energy, Culham Science Centre, Abingdon, Oxon, OX14 3DB, United Kingdom
[5] Pacific Northwest National Laboratory, Richland WA, United States of America
[6] Department of Physics, University of Helsinki, PO Box 43, FI-00014 Helsinki, Finland
[7] Massachusetts Institute of Technology, Cambridge, MA, United States of America
[8] Japan Atomic Energy Agency, Tokai-mura, Naka-gun, Ibaraki-ken, Japan
[9] University of Tennessee-Knoxville, Knoxville, TN, United States of America

E-mail: jmarian@ucla.edu

Received 13 July 2016, revised 7 December 2016
Accepted for publication 16 December 2016
Published 9 June 2017

Abstract

Under the anticipated operating conditions for demonstration magnetic fusion reactors